Geothermics 117 (2024) 102888

Contents lists available at ScienceDirect

Geothermics

journal homepage: www.elsevier.com/locate/geothermics

Comparison of the thermal and hydraulic performance of single U-tube, double U-tube and coaxial medium-to-deep borehole heat exchangers

Christopher S. Brown *, Isa Kolo, David Banks, Gioia Falcone

James Watt School of Engineering, University of Glasgow, Glasgow G12 8QQ, United Kingdom

ARTICLE INFO

Keywords:
Single U-tube
Double U-tube
Coaxial
Borehole heat exchanger
OpenGeoSys
Middle-deep
Deep
DBHE

ABSTRACT

Decarbonisation of heat is essential in curbing carbon dioxide emissions and can be achieved through the use of geothermal systems. Recently, single-well, closed-loop, deep borehole heat exchangers, using a coaxial design, have become the focus of attention, partly due to the potential to repurpose existing infrastructure (such as oil and gas wells); however, few have investigated the potential for other types of heat exchanger for middle-deep geothermal systems. Therefore, in this study, a comprehensive numerical analysis was undertaken using OpenGeoSys software to investigate the thermal and hydraulic performance of coaxial, single U-tube and double U-tube middle-deep borehole heat exchangers (MDBHEs). The purpose of this paper is to test the maximum operational depth for each type of pipe configuration as few wells have been completed to depths exceeding 500 m using single/double U-tube configurations. The best performing MDBHEs should minimise parasitic and hydraulic losses, whilst maximising thermal output. Furthermore, ground sourced heat pumps require electricity; therefore, at times where electricity prices are high (and drilling costs can be minimised) it may be more beneficial to utilise MDBHEs to encounter greater temperatures.

Results indicate that coaxial MDBHEs provide the best performance in terms of specific heat extraction and lowest pressure/parasitic losses. Double U-tube MDBHEs can provide a similar thermal performance to the coaxial design, but have significantly greater hydraulic pressure losses across all simulations, which translates to greater parasitic pumping power costs. Single U-tube MDBHEs demonstrate the poorest performance in terms of heat extraction and pressure losses. At the end of the 25-year base case scenario for a 800 m MDBHE, coaxial, U-tube and double U-tube configurations, all with a fluid circulation rate of 5 L/s, provided specific heat extraction rates of 39.1 W/m, 32.8 W/m, and 36.0 W/m, respectively, with the fluid inlet temperature set as a constant of 5 °C. For these simulations, pressure losses were estimated as 85 kPa (coaxial), 1.46 MPa (single U-tube) and 423 kPa (double U-tube)—the single U-tube value being close to the nominal 16 bar (1.6 Mpa) pressure rating of SDR11 high density polyethylene pipe. Further parametric analysis was also undertaken, investigating depth, flow rate, rock thermal conductivity, pipe diameter and shank spacing.

1. Introduction

Decarbonisation of heat is essential to meeting net zero carbon emission targets. Various methods of decarbonisation of heat exist, including solar thermal, deep geothermal, air-sourced heat pumps, and closed- or open-loop ground sourced heat pump systems. In recent years, research has focused on the potential for deep borehole heat exchangers (DBHEs) to i) meet heating demand (e.g., Falcone et al., 2018; Chen et al., 2019; Brown et al., 2021; Doran et al., 2021; Gascuel et al., 2022; Brown and Howell., 2023; Kolo et al., 2023), ii) meet heating and cooling demand (e.g., Zhao et al., 2022; Zhang et al., 2022a), and iii) include a component of thermal energy storage (e.g., Schulte et al., 2016; Xie et al., 2018; Qin et al., 2022; Brown et al., 2023a,b). Typically, the coaxial design of a DBHE is used in deeper systems to avoid the large hydraulic pressure losses and installation difficulties associated with U-tubes (Deng et al., 2019).

DBHE systems have been comprehensively investigated in literature. Engineering and geological parameters can impact the performance of heat extraction: i) Increased flow rates, up to an optimal point, have been shown to correspond to greater thermal power outputs by reducing the temperature differential and thus the internal thermal interference between downflowing and upflowing fluid streams (Kohl et al., 2002;

* Corresponding author.
E-mail address: christopher.brown@glasgow.ac.uk (C.S. Brown).

https://doi.org/10.1016/j.geothermics.2023.102888
Received 4 August 2023; Received in revised form 14 November 2023; Accepted 26 November 2023
Available online 7 December 2023

Nian et al., 2019; Li et al., 2021), ii) coaxial design parameters (i.e., radius of inner and outer pipes) can lead to higher outlet temperatures by increasing the velocity in the central pipe and reducing the velocity in the annular space (e.g., Wang et al., 2017), iii) thermal conductivity of the surrounding rocks will govern the rate of heat extraction (e.g., Kohl et al., 2000; Fang et al., 2018), iv) natural convection (Bidarmaghz and Narsilio, 2022) and regional groundwater flow can improve performance, but it is unlikely that sufficient velocities will be encountered at depth (Brown et al., 2023b), v) increased depth will significantly improve the rate of thermal extraction (e.g., Holmberg et al., 2016; Song et al., 2018; Xia et al., 2021; Zhang et al., 2021), vi) the mode of operation (i.e. downflow in annulus versus downflow in axial pipe) can influence DBHE performance (e.g., Cai et al., 2019; Luo et al., 2022; Perser and Frigaard, 2022; Brown et al., 2023c), vii) higher geothermal gradients lead to an increase in outlet temperatures and achievable thermal power (Pan et al., 2019), and viii) if developed in an array of DBHEs, the design is important to minimise thermal interaction (Holmberg et al., 2015; Cai et al., 2021, 2022; Zhang et al., 2022b).

Coaxial DBHEs operate in heat extraction mode by circulating a cool fluid downwards through the annular space (Figs. 1 and 2). The fluid warms with increasing depth under the natural geothermal gradient from conduction with the borehole wall, before being pumped back to the surface via the central pipe at a faster velocity to minimise heat losses through thermal short circuiting. U-tube and double U-tubes, which are typically used for shallow projects (Figs. 1 and 2), circulate a water-based heat transfer fluid down and up the hole; in this case, the arrangement is usually laterally symmetrical, with fluid descending via a circular pipe, and then ascending via an upflow pipe (shank) of the U-tube of an identical diameter. A double U-tube comprises two single U-tubes effectively connected in parallel (i.e., two downhole shanks and two upflow shanks). U-tubes tend to be made of high density or cross-linked polyethylene (HDPE or PEX) with SDR11 wall thickness (with a nominal burst pressure of 16 bar) being a typical specification (in Sweden, SDR 17 has been common for shallower closed loop boreholes, but Olsson (2018a) recommends SDR11 for deeper boreholes). Standard outer diameters (OD) of polyethylene pipe used in U-tube systems are typically 32, 40, 50 mm, although 63 mm OD can also be regarded as a feasible diameter. At least one company produces a 45 mm OD variant, with rifled interior (Muovitech, 2023). While coaxial systems typically (but not necessarily) occupy the entire borehole, U-tubes are either suspended within the column of natural groundwater filling the borehole (which provides a thermal contact between the U-tube and borehole wall, and within which conductive and convective heat transfer can occur), or they can be sealed in the borehole by a low permeability backfill or "grout". This grout can be cement-based or a mixture of fine silica sand and bentonite, and should have an enhanced thermal conductivity (>1.5 W/m/K).

In shallow systems, comparisons between coaxial and U-tube borehole heat exchangers have been made, which focus either on the model design itself (e.g., Gordon et al., 2017) or on short-term thermal response tests (e.g., Harris et al., 2022; Morchio et al., 2022). Past work has shown that the coaxial design provides a better heat transfer capacity (Wang, 2014). However, few studies have extended the comparison to monitor hydraulic and thermal performance in deeper systems for the lifetime of a borehole heat exchanger. Whilst it is commonly accepted that coaxial systems will be employed at depths of over 1 km due to the practical difficulties of U-tube system construction in deeper boreholes (Olsson, 2018c; Deng et al., 2019), there is limited research on medium-to-deep borehole heat exchangers (MDBHEs) and the implications of using different types of configurations (i.e., U-tube,

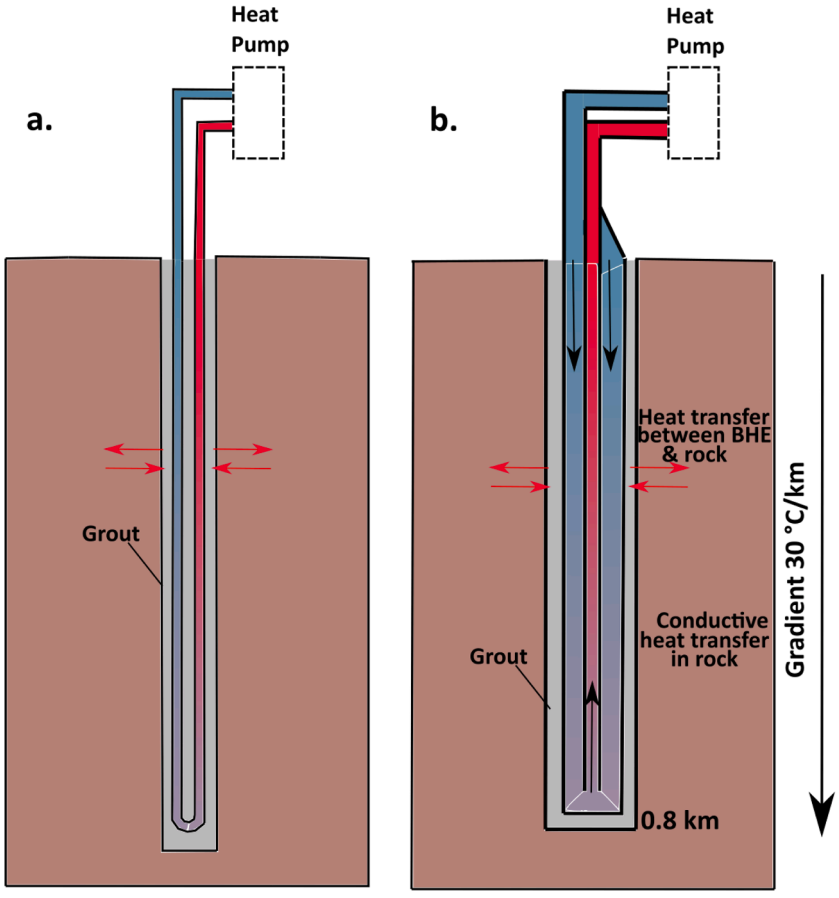

Fig. 1. Schematic of different types of MDBHE configuration, with (a) U-tube and (b) coaxial designs. Note that a double U-tube configuration would consist of two U-tubes within the borehole similar to design (a).

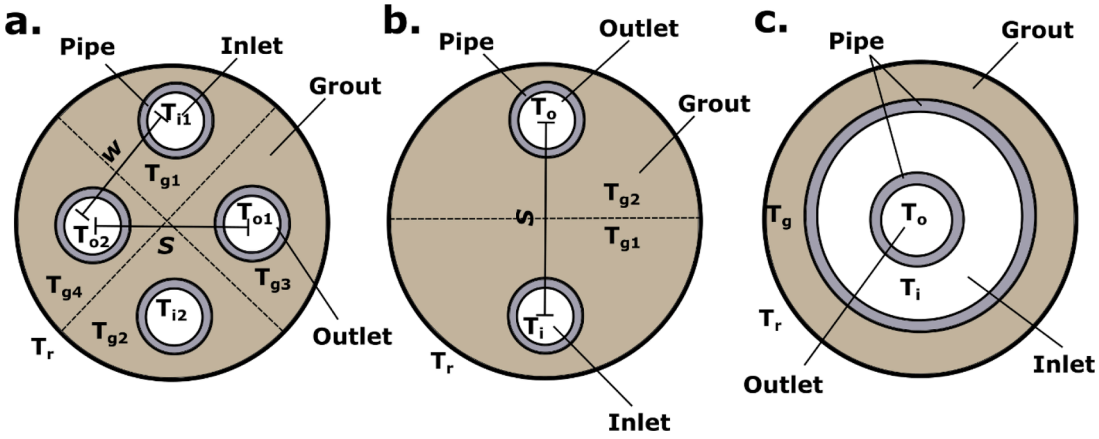

Fig. 2. Schematic of cross sections of different types of MDBHE configuration, for (a) double U-tube, (b) single U-tube and (c) coaxial designs. Temperatures (*T*) are shown for the rock—subscript *r*; inlet(s)—subscript i; outlet(s)—subscript *o*; and grout zone(s)—subscript *g*. It is worth noting that the "grouted" section in the single and double U-tubes could be filled with groundwater, but in this study it is modelled as a thermally enhanced grout material. When calculating the distance between shanks for the double U-tube, the open-source finite element software, OpenGeoSys (OGS), employed in the study, uses the centre-to-centre spacing between adjacent tubes (*w*) (i.e., distance between T_{i2} and T_{o1}). However, the shank spacing values listed in this paper for double U-tubes is based on the centre-to-centre diagonal spacing between pipes (i.e., (*S*) as shown in figure 'a' and 'b').

double U-tube and coaxial—Fig. 2) on heat transfer efficiency, pressure changes and parasitic losses.

1.1. Defining middle-deep borehole heat exchangers

Breede et al. (2015) and others (Homuth et al., 2016) have suggested that medium-to-deep (or middle-deep) geothermal systems span the depth range from 400 m to 1000 m depth, yet others suggest that "shallow" should be classified as depths less than 500 m due to government regulations on renewable heat incentive classifications (Watson et al., 2020). In the UK, the Infrastructure Act (2015) imposes different rules and rights for "deep" geothermal systems >300 m, so there is ambiguity over the lower cut offs of such systems. In this paper, the depth range of 500 m to 1000 m was defined for middle-deep geothermal systems, in line with both UK based renewable heat incentives (Watson et al., 2020) and previous classifications (Breede et al., 2015; Homuth et al., 2016). Although others have also defined the middle-deep to range from 1500 m to 3000 m (Bao et al., 2023; Zhang et al., 2023), this depth range would be considered as a DBHE in this paper.

1.2. Evaluation of middle-deep borehole heat exchangers in practice

In many European nations, the typical depth of closed loop borehole heat exchangers (BHE) has steadily been increasing. In the UK around 10–15 years ago, a typical U-tube BHE would have been installed to ~100 m depth (Banks 2012); today, grouted BHEs are commonly constructed to 150–200 m depth. In Sweden, the average BHE depth increased from 100 to 171 m between 1995 and 2013 (Gehlin et al., 2016; Olsson 2018a). U-tube based BHEs in the depth range 200 to 300 m are common in Scandinavia (Gehlin et al., 2016, 2020), where they are usually suspended in the natural groundwater column (no grouting). Olsson (2018a) and Gehlin et al. (2020) cite U-tube diameters of 45–50 mm OD as typical for BHE of around 300 m depth.

Relatively deep BHEs are constructed in large arrays to serve large commercial or public sector heat demands. 228 BHEs to a depth of 200 m serve Akershus Hospital, Norway, while 204 BHEs to 240–250 m depth supply Karlstad University campus, Sweden (Gehlin et al., 2016). Several arrays comprising 215 BHEs to an average depth of 270 m were installed to serve the Volvo Powertrain plant in Köping, Sweden (Wirtén 2017; Gehlin et al., 2020). Korhonen et al. (2018) analyse the performance of an array of 157 BHEs to a modal depth of 300 m using 40 mm diameter U-tube collectors suspended in water-filled 140 mm diameter boreholes, at Sipoo, Southern Finland. As early as 2011, Swedish drillers were installing BHEs to depths of 400–500 m, and between 2011 and 2018, one contractor drilled 150 BHEs between 400 and 601 m depth (Olsson 2018a). At Drammen in Norway, a school is heated by 5 BHEs to 500 m depth, each installed as single U-tubes of 50 mm outer diameter within 140 mm diameter boreholes (Gehlin et al., 2016). Mazzotti et al. (2018) document an array of four 510 m BHEs comprising 50 mm outer diameter polyethylene U-tubes of SDR17 (SDR11 in upper 150 m) supplying two buildings of 29 apartments in central Stockholm. They also discuss an array of 22 grouted U-tube BHEs to 335 m depth in Uppsala, Sweden.

Significantly-sized arrays of coaxial MDBHEs are also being installed in Europe, such as the arrays of 800 m deep boreholes forming part of the Métamorphose Project in Lausanne, Switzerland (Olsson, 2018b) at Plains-du-Loup (SiL, 2023). The initial trial BHEs in Lausanne were 750 m deep boreholes installed with double U-tubes of 50 mm outer diameter in high pressure PN80 pipe (Gehlin et al., 2016). Olsson (2018b) cites Nicolas de Varreux of the Lausanne project, who claims that installing "traditional" U-tubes beyond 500 m does not give increased energy returns. De Varreux (Olsson 2018b) claims that a U-tube to 800 m yields no greater energy yield than one to 500 m, due the increased parasitic pumping power required by the increased hydraulic losses in circulation. He thus champions coaxial system at depths greater than 500 m and this informed the eventual decision to use coaxial BHEs in the 140 boreholes planned at Lausanne (SiL, 2023). Olsson (2018c) also cites Henrik Holmberg's conclusion that, in Norway, one can use U-tube systems of large diameter down to around 500 m but, beyond that depth, only coaxial systems result in increased net efficiency.

With increasing depth, the installation of BHEs (and especially U-tubes) face progressively greater geotechnical and engineering challenges in installation. In Scandinavia, for example, the cost-effective depth of drilling in hard rock has been limited by the available size of compressors that could be used with the commonly-utilised compressed air down-the-hole hammer rigs. A Swedish drilling contractor noted (Olsson 2018a) that difficulties in lifting water and cuttings from boreholes increase significantly below 300 m. In recent years, larger compressors and innovations in drilling (e.g., water-hammer rigs) have increased the economically viable depth (Gehlin et al., 2016). In the hard metamorphic and igneous lithologies characteristic of Scandinavia, the completed borehole is stable, without the need for anything other than superficial casing, rendering installation of heat exchangers in a groundwater-filled borehole relatively unproblematic. In the softer sedimentary sequences elsewhere in Europe, deep drilling has often

either required (expensive) casing, or drilling operations involving mud-systems, to maintain an open bore while the BHE and thermally enhanced grout are emplaced.

Naturally, the difficulties involved in the emplacement of a 500 m string of U-tube in a borehole will be significantly greater than those with a 100 m string. The frictional resistance against the borehole walls will be greater; the U-tube will need to be filled and pressurised with a fluid of appropriate density and also weighted in order to ensure that it has neither unwanted buoyancy relative to the borehole fluid (mud or natural groundwater), nor excessive weight, which could damage the pipe. As natural groundwater salinity and density increase with borehole depth, the challenge of achieving the correct U-tube buoyancy and pressure becomes increasingly problematic. A coaxial pipe (which is open to the borehole fluid) is arguably less problematic to install.

Olsson (2018a) notes that, in deeper boreholes, the density of drilling mud or grout outside a U-tube during emplacement can exert a huge pressure differential on the tube, risking the collapse of the polyethylene pipe, if it is not carefully pre-pressurised prior to installation. Gehlin et al. (2016) notes that multi-stage grouting operations may be required to maintain acceptable pressure differentials. Gehlin et al. (2016) note that a risk of U-tube pipe collapse can even occur when a low-density heat transfer fluid (e.g., ethanol solution) is used in a deep groundwater-filled borehole, especially if the deep groundwater is dense and saline. Gehlin et al. (2016) also note that the collapse pressure of HDPE pipe is much less than the burst pressure: a mere 1.4 bar for SDR17 pipe and 5.7 bar for SDR11. Gehlin et al. (2016) finally recommend that consideration should be made for expansion and contraction of long lengths of plastic U-tube due to heating and cooling during operation.

Both Wirtén (2018) and Olsson (2018a) clarify the advantages and disadvantages of progressively deeper BHE. On the positive side, the amount of electricity used by a heat pump typically decreases by 5 % for every additional °C in the fluid return temperature from the BHE. They note that the main challenge with deep BHEs is the increasing hydraulic pressure losses with fluid circulation through greater lengths of pipe (and as the borehole gets deeper, the potential heat recovery increases, requiring greater fluid flow rates as well as longer pipe circuits). They conclude that, for deeper BHEs, coaxial systems perform most efficiently. They also note that, with deeper boreholes, the degree of thermal interference between upflow and downflow fluid flows increases, eroding the thermal efficiency of the system. This in turn, implies that adequate shank spacing becomes more important with deeper U-tubes, adding to installation difficulty. Gehlin et al. (2016) provide a chart quantifying the increase in borehole thermal resistance with depth. Mazzotti et al. (2018) report a relatively high borehole thermal resistance of 0.21 Km/W being derived from a thermal response test in an 800 m deep coaxial borehole (Asker, Norway), albeit at a limited flow rate (c. 1.5 L/s at 15 kW) and unfavourable flow direction. Mazzotti et al. (2018) document the results of thermal response testing of the 335 m deep U-tube BHE in Uppsala, Sweden. Borehole thermal resistances were estimated before (groundwater-filled bore) and after grouting: the results were somewhat variable, but tended to be around 0.1 Km/W.

Wirtén (2018), Mazzotti et al. (2018) and Olsson (2018c) report trials of coaxial BHEs carried out on two 800 m boreholes in Asker, Norway. The trials demonstrated that coaxial configurations resulted in significantly lower hydraulic pressure losses than in conventional U-tube systems. The trials concluded that up to 70 % of the recovered heat energy was subject to internal thermal short circuiting, however, and recommended the development of insulated coaxial pipes to minimise internal thermal short circuiting. Wirtén (2018) notes that the efficiency of conventional insulation materials tends to be compromised by fluid pressure compression; the study suggests that a double-skinned internal pipe, with an insulating air layer, would be an attractive solution. Holmberg (2016a) concluded, however, that the optimum solution for DBHE is a "coaxial BHE with a thin-walled centre pipe, which is operated with a high mass flow rate": this keeps costs low, hydraulic resistance low and also reduces thermal interference, as the high flow rate minimises temperature differential between upward and downward fluid fluxes. Holmberg et al. (2016b) further notes that, with increasing depth, borehole diameter can be increased (albeit at extra cost) to keep hydraulic pressure losses within reasonable bounds. Olsson (2018c) reports that, following the 800 m Asker coaxial BHE trials, two 1500 m deep boreholes have been constructed at Oslo's Gardermoen Airport, which will be used for snow-melting (without a heat pump).

Coaxial boreholes are often completed in Scandinavia as open, uncased boreholes (with only necessary surface casing to exclude superficial and weathered materials) where annular fluid flow circulates directly against a hard rock wall. Alternatively, boreholes may be completed with a thin flexible outer plastic liner resting against the rock wall (Mazzotti et al., 2018; Triopipe Geotherm 2023). In non-"hard rock" countries, such as the UK, it is arguably more common for a borehole to be cased with steel casing to greater depths in order to stabilise the borehole wall. The annulus behind the casing will usually be at least partially filled with a grout cement to prevent fluid flow behind the casing and unwanted connection of aquifer horizons (e.g., Kolo et al., 2023). Heat transfer to the annular fluid inside the borehole thus takes place through layers of both cement grout and steel. Where the borehole is fully lined or cased, one could arguably circulate an anti-freeze solution (ethanol or glycol) to permit fluid temperatures to fall below 0 °C, although the increased viscosity would result in significantly higher-pressure losses. For this reason, water is often used as the heat transfer fluid in coaxial MDBHE, especially if the borehole wall is unlined (most environmental authorities would view unfavourably any possibility of leakage of anti-freeze to the natural groundwater environment).

Olsson (2018a) notes that several Swedish geothermal collector pipe manufacturers are developing coaxial geothermal installations which do not need to be an integral part of the borehole design, but which can be installed in a completed borehole in much the same way as a U-tube (Triopipe Geotherm 2023).

1.3. Objectives of the study

As highlighted in the comprehensive literature review of operating BHEs in the middle-deep geothermal system range there are still unanswered questions in terms of the suitability of BHE configurations over depths of 500 m. As a result, in this study, a comprehensive analysis was undertaken to evaluate the thermal and hydraulic performance of different MDBHE configurations among a range of parameters over the lifetime of a system. Models were developed using OpenGeoSys (OGS) to simulate the different MDBHE types. Initial validation was conducted against two different thermal response tests to demonstrate the accuracy of the models against real data, before testing if different parameters can influence the suitability of MDBHE configurations. A range of thermal conductivities were modelled to cover a vast range of geological settings (i.e., sedimentary, metamorphic and igneous) to have a wide applicability.

The key aims were to evaluate some of the key questions highlighted from literature: i) can single and double U-tube MDBHEs be operated efficiently, in terms of parasitic losses in contrast to the thermal power, at depths >500 m, ii) what parameters can ensure efficient performance of MDBHES, and iii) is it possible to compare the impact of different parameters on thermal and hydraulic performance of MDBHEs? Historically the geothermal sector has been focussed on electricity generation from deep systems, while shallow geothermal developments have focussed on minimising drilling and installation costs. This has left a void in middle-deep systems which can aid in decarbonising space heating. Furthermore, ground sourced heat pumps require electricity, therefore, at times where electricity prices are high it may be more beneficial to drill deeper to encounter greater temperatures. Additionally, if drilling in hard-rock (i.e., granite) and the hole is left 'open' (i.e. no casing), costs can be reduced, making MDBHEs a more suitable

alternative (Banks, 2023). This paper, therefore, provides a thorough novel assessment of closed-loop MDBHEs to analyse the potential of various configurations.

2. Methods

The borehole heat exchanger heat transport module of OGS was adopted in this study. The tool implements the 'Dual-continuum' approach which idealises the MDBHE as a one-dimensional continuum (meshed using line elements) surrounded by a three-dimensional rock formation (meshed using prism elements). OGS can simulate several MDBHE pipe configurations, including coaxial pipe (both annular inlet - CXA and central pipe inlet - CXC), single-U pipe (1 U), double-U pipe (2 U), and a simple (grouted, non-concentric) pipe (1P). The model considers heat transfer in (a) the rock formation - conduction and convection, (b) the grout region(s) - conduction, and (c) the inlet pipe(s) and outlet pipe(s) - convection. In this work, no groundwater flow was considered for the formation as it has been proven to have limited impact under low Darcy velocities and with relatively thin aquifers (Chen et al., 2019; Brown et al., 2023b); hence, heat transfer in the formation is governed by conduction only.

2.1. Governing equations for conduction in the subsurface rock

The energy balance for the rock formation considering conduction only is given by (Hein et al., 2016; Chen et al., 2019; Kolo et al., 2022):

$$\frac{\partial}{\partial t}\left[\phi\rho_f c_f + (1-\phi)\rho_r c_r\right]T_r - \nabla\cdot(\Lambda_r\cdot\nabla T_r) = H_r \tag{1}$$

in which ϕ is the rock porosity, ρ_f and c_f are the density and specific heat capacity of the heat transfer fluid, respectively, ρ_r and c_r are density and specific heat capacity of the rock, respectively, T_r is the temperature of the rock, H_r is the source term and Λ_r is the thermal hydrodynamic dispersion tensor. A Neumann-type boundary condition is adopted in which the heat flux between the DBHE and rock formation, q_{nT_r}, is given by:

$$q_{nT_r} = -(\Lambda_r\cdot\nabla T_r) \tag{2}$$

It is also possible to impose Dirichlet-type or Cauchy-type boundary conditions (Diersch et al., 2011).

2.2. Governing equations for middle-deep borehole heat exchangers

The governing equations for the grout, inlet and outlet pipes depend on the MDBHE pipe configuration being considered. In addition to the governing equation for the rock, a coaxial pipe will have 3 governing equations for the 3 components: 1 inlet (annulus), 1 outlet (central) pipe, and 1 grout zone. Here, the governing equations for the CXA configuration of the coaxial pipe, with the annulus as inlet and the central pipe as outlet, are presented. A 1 U pipe has 4 additional components and hence 4 governing equations: 1 inlet pipe, 1 outlet pipe, and 2 grout zones (i.e., the grout zones around each pipe). The 2 U pipe has 2 inlet pipes, 2 outlet pipes, and 4 grout zones, and hence 8 governing equations (refer to Fig. 2).

2.2.1. Coaxial

The heat transport equations for 1 inlet (annulus) (subscript *i*), 1 outlet (central) pipe (subscript *o*), and 1 grout zone (subscript *g*) (see Figs. 1 and 2) along with the corresponding boundary conditions are as follows (Diersch et al., 2011a; Hein et al., 2016; Chen et al., 2019; Kolo et al., 2022):

Inlet:

$$\rho_f c_f\frac{\partial T_i}{\partial t} + \rho_f c_f \boldsymbol{v}\cdot\nabla T_i - \nabla\cdot(\Lambda_f\cdot T_i) = H_i \tag{3}$$

with boundary condition,

$$q_{nT_i} = -\Phi_{fig}(T_r - T_i) - \Phi_{ff}(T_o - T_i) \tag{4}$$

where the subscript *i* indicates inlet and *o* indicates outlet; $\boldsymbol{v}$ is the fluid velocity vector. Φ is the heat transfer coefficient, which is a function of thermal resistance between components, Φ_{fig} is the heat transfer coefficient between the grout and the inlet pipe, and Φ_{ff} is the heat transfer coefficient between the inlet pipe and the outlet pipe.

Outlet pipe:

$$\rho_f c_f\frac{\partial T_o}{\partial t} + \rho_f c_f \boldsymbol{v}\cdot\nabla T_o - \nabla\cdot(\Lambda_f\cdot T_o) = H_o \tag{5}$$

with boundary condition,

$$q_{nT_o} = -\Phi_{ff}(T_i - T_o) \tag{6}$$

Grout zone:

$$(1-\phi_g)\rho_g c_g\frac{\partial T_g}{\partial t} - \nabla\cdot\left[(1-\phi_g)\lambda_g\cdot\nabla T_g\right] = H_g \tag{7}$$

with boundary condition,

$$q_{nT_g} = -\Phi_{gr}(T_r - T_g) - \Phi_{fig}(T_i - T_g) \tag{8}$$

Here, the subscript *g* represents grout. λ_g is the thermal conductivity of the grout, and Φ_{gr} is the heat transfer coefficient between the rock formation and grout.

2.2.2. U-tube

The heat transfer equations for 1 inlet pipe (subscript *i*), 1 outlet pipe (subscript *o*), 2 grout zones (subscripts *g*1 and *g*2), and boundary conditions are summarised below. As shown in Fig. 2, the grout zone is divided into two equal parts, with the inlet pipe surrounded by grout zone 1 and the outlet pipe surrounded by grout zone 2. The equations are (Diersch et al., 2011a; Hein et al., 2016):

Inlet pipe:

$$\rho_f c_f\frac{\partial T_i}{\partial t} + \rho_f c_f \boldsymbol{v}\cdot\nabla T_i - \nabla\cdot(\Lambda_f\cdot T_i) = H_i \tag{9}$$

with boundary condition,

$$q_{nT_i} = -\Phi_{fig}^{1U}(T_{g1} - T_i) \tag{10}$$

in which Φ_{fig}^{1U} is the heat transfer coefficient between the inlet pipe and grout zone 1 for a 1 U pipe.

Outlet pipe:

$$\rho_f c_f\frac{\partial T_o}{\partial t} + \rho_f c_f \boldsymbol{v}\cdot\nabla T_o - \nabla\cdot(\Lambda_f\cdot T_o) = H_o \tag{11}$$

with boundary condition,

$$q_{nT_o} = -\Phi_{fog}^{1U}(T_{g2} - T_o) \tag{12}$$

in which Φ_{fog}^{1U} is the heat transfer coefficient between the outlet pipe and grout zone 2 for a 1 U pipe.

Grout zone 1:

$$(1-\phi_g)\rho_g c_g\frac{\partial T_{g1}}{\partial t} - \nabla\cdot\left[(1-\phi_g)\lambda_g\cdot\nabla T_{g1}\right] = H_{g1} \tag{13}$$

with boundary condition,

$$q_{nT_{g1}} = -\Phi_{gr}^{1U}(T_r - T_{g1}) - \Phi_{fig}^{1U}(T_i - T_{g1}) - \Phi_{gg}^{1U}(T_{g2} - T_{g1}) \tag{14}$$

in which T_{g1} is the temperature at grout zone 1 and T_{g2} is the temperature at grout zone 2. The heat transfer coefficient Φ_{gr}^{1U} is between the

grout and the rock and Φ_{gg}^{1U} is between grout zone 1 and grout zone 2, both for a 1 U pipe.

Grout zone 2:

$$(1-\phi_g)\rho_g c_g \frac{\partial T_{g2}}{\partial t} - \nabla\cdot\left[(1-\phi_g)\lambda_g\cdot\nabla T_{g2}\right] = H_{g2} \tag{15}$$

with boundary condition,

$$q_{nT_{g2}} = -\Phi_{gr}^{1U}\left(T_r - T_{g2}\right) - \Phi_{fog}^{1U}\left(T_o - T_{g2}\right) - \Phi_{gg}^{1U}\left(T_{g1} - T_{g2}\right) \tag{16}$$

2.2.3. Double U-tube

The 2 U tube has 2 inlets (subscripts $i1$ and $i2$), and 2 outlets (subscripts $o1$ and $o2$), and the grout zone is divided into four equal quadrants (subscripts $g1$, $g2$, $g3$ and $g4$) for analysis (see Fig. 2). Hence, there are 8 governing equations and boundary conditions with interactions between components following a similar approach as the 1 U pipe. Grout zones $g1$ and $g2$ are associated with inlets $i1$ and $i2$ respectively while grout zones $g3$ and $g4$ are associated with outlets $o1$ and $o2$, respectively. The resulting governing equations are presented next (Diersch et al., 2011a):

2 inlet pipes:

$$\rho_f c_f \frac{\partial T_k}{\partial t} + \rho_f c_f \boldsymbol{v}\cdot\nabla T_k - \nabla\cdot\left(\Lambda_f\cdot T_k\right) = H_k \text{ in } \Omega_k \text{ for } k = i1, i2 \tag{17}$$

with boundary conditions,

$$q_{nT_{i1}} = -\Phi_{fig}^{2U}\left(T_{g1} - T_{i1}\right) \text{ on } \Gamma_{i1} \tag{18}$$

$$q_{nT_{i2}} = -\Phi_{fig}^{2U}\left(T_{g2} - T_{i2}\right) \text{ on } \Gamma_{i2} \tag{19}$$

In the preceding equations, Ω is the domain and Γ is the domain boundary for the 2 U tube. Φ_{fig}^{2U} is the heat transfer coefficient between inlet pipe 1 and grout zone 1. It remains the same between inlet pipe 2 and grout zone 2.

2 outlet pipes:

$$\rho_f c_f \frac{\partial T_k}{\partial t} + \rho_f c_f \boldsymbol{v}\cdot\nabla T_k - \nabla\cdot\left(\Lambda_f\cdot T_k\right) = H_k \text{ in } \Omega_k \text{ for } k = o1, o2 \tag{20}$$

with boundary conditions,

$$q_{nT_{o1}} = -\Phi_{fog}^{2U}\left(T_{g3} - T_{o1}\right) \text{ on } \Gamma_{i1} \tag{21}$$

$$q_{nT_{o2}} = -\Phi_{fog}^{2U}\left(T_{g4} - T_{o2}\right) \text{ on } \Gamma_{i2} \tag{22}$$

where Φ_{fog}^{2U} is the heat transfer coefficient between the outlet pipe and the grout zone, i.e. between $o1$ and $g3$, and also between $o2$ and $g4$

4 grout zones:

$$(1-\phi_g)\rho_g c_g \frac{\partial T_k}{\partial t} - \nabla\cdot\left[(1-\phi_g)\lambda_g\cdot\nabla T_k\right] = H_k \text{ in } \Omega_k \text{ for } k = g1, g2, g3, g4 \tag{23}$$

with boundary conditions,

$$\begin{aligned} q_{nT_{g1}} = &-\Phi_{gr}^{2U}\left(T_r - T_{g1}\right) - \Phi_{fig}^{2U}\left(T_{i1} - T_{g1}\right) - \Phi_{gg2}^{2U}\left(T_{g2} - T_{g1}\right) \\ &- \Phi_{gg1}^{2U}\left(T_{g3} - T_{g1}\right) - \Phi_{gg1}^{2U}\left(T_{g4} - T_{g1}\right) \text{ on } \Gamma_{g1} \end{aligned} \tag{24}$$

$$\begin{aligned} q_{nT_{g2}} = &-\Phi_{gr}^{2U}\left(T_r - T_{g2}\right) - \Phi_{fig}^{2U}\left(T_{i2} - T_{g2}\right) - \Phi_{gg2}^{2U}\left(T_{g1} - T_{g2}\right) \\ &- \Phi_{gg1}^{2U}\left(T_{g3} - T_{g2}\right) - \Phi_{gg1}^{2U}\left(T_{g4} - T_{g2}\right) \text{ on } \Gamma_{g2} \end{aligned} \tag{25}$$

$$\begin{aligned} q_{nT_{g3}} = &-\Phi_{gr}^{2U}\left(T_r - T_{g3}\right) - \Phi_{fog}^{2U}\left(T_{o1} - T_{g3}\right) - \Phi_{gg2}^{2U}\left(T_{g4} - T_{g3}\right) \\ &- \Phi_{gg1}^{2U}\left(T_{g1} - T_{g3}\right) - \Phi_{gg1}^{2U}\left(T_{g2} - T_{g3}\right) \text{ on } \Gamma_{g3} \end{aligned} \tag{26}$$

$$\begin{aligned} q_{nT_{g4}} = &-\Phi_{gr}^{2U}\left(T_r - T_{g4}\right) - \Phi_{fog}^{2U}\left(T_{o2} - T_{g4}\right) - \Phi_{gg2}^{2U}\left(T_{g3} - T_{g4}\right) \\ &- \Phi_{gg1}^{2U}\left(T_{g1} - T_{g4}\right) - \Phi_{gg1}^{2U}\left(T_{g2} - T_{g4}\right) \text{ on } \Gamma_{g4} \end{aligned} \tag{27}$$

in which Φ_{gr}^{2U} is the heat transfer coefficient between the surrounding rock and the grout zone for the 2 U tube assumed to remain the same for all four grout zones.Φ_{gg1}^{2U} is the heat transfer coefficient between an inlet pipe's grout zone and an outlet pipe's grout zone, i.e. between (a) $g1$ and $g4$, (b) $g1$ and $g3$, (c) $g2$ and $g3$, and (d) between $g2$ and $g4$. Φ_{gg2}^{2U} is the heat transfer coefficient between two inlet pipe grout zones (between $g1$ and $g2$) or two outlet pipe grout zones (between $g3$ and $g4$). The detailed procedure for calculating thermal resistances and the relationship between heat transfer coefficients and thermal resistances can be found in Diersch et al. (2011a). Eqs. (1) and (2) are solved together with Eqs. (3)–(8) for coaxial pipe, with Eqs. (9)–(16) for a 1 U pipe and with Eqs. (17)–(27) for a 2 U pipe. The governing equations are discretised using their weak forms. As stated earlier, the finite element implementation of these equations in OGS is used in this work.

2.3. Evaluating pressure drop and power consumption from the circulation pump

To compute the pressure drop (ΔP) in the MDBHE (i.e., the pressure difference between the BHE inlet and BHE outlet), the sum of the pressure drops in the downflow and upflow sections of the BHE was calculated (in the case of a coaxial BHE, the downflow section is a circular annular space, rather than a circular pipe). The ΔP was determined using the Darcy-Weisbach equation with Petukhov's relation for the friction factor (Petukhov 1970; Incropera et al., 2007; Chen et al., 2019):

$$\Delta P = \frac{L\rho_f v_f^2}{2D_h[0.79\ln(Re) - 1.64]^2} \tag{28}$$

in which $L$is the length of the pipe, v_f is the mean fluid velocity of the inlet or outlet as considered, D_h is the hydraulic diameter and Re is the turbulent flow Reynolds number. The hydraulic diameters can be calculated as a function of the diameter/radius of outer and inner pipes (see Engineering Toolbox, 2023) The equation assumes turbulent flow in all pipe regions. The equation only calculates the pressure losses in the straight-line portions of the pipes and ignores pressure losses associated with bends, fittings, joints and any surface heat exchanger. Fluid properties were assumed as given in Table 1.

The electrical power consumption of the circulation pump (W_{cp}) required to overcome the pipe frictional losses was calculated as (e.g., Liu et al., 2019):

$$W_{cp} = \frac{\Delta P \times Q}{n} \tag{29}$$

where ΔP is the pressure drop in the DBHE, Q is the mass flow rate and n is the overall efficiency of the electrical-to-hydraulic power conversion in the circulation pump (assumed to be 60 %). Note that the heat

Table 1
Base case parameters. Note the flow rate for each case is split for the double U-tube, so each pipe has half the flow rate input to the system.

Parameter	Value	Units
Borehole diameter	216	mm
Borehole length	800	m
Saturated ground thermal conductivity	2.5	W/(m K)
Saturated ground volumetric heat capacity	1.9×10^6	J/(K m^3)
Water flow rate	5	L/s
Water density	998	kg/m^3
Water volumetric heat capacity	4.179×10^6	J/(K m^3)
Water thermal conductivity	0.59	W/(m K)
Dynamic water viscosity	8×10^{-4}	kg/(m s)
Basal heat flow	75	mW/m^2
Geothermal gradient	30	°C/km
Surface temperature	9	°C
Grout thermal conductivity	1.05	W/(m K)
Grout volumetric heat capacity	1.2×10^6	J/(K m^3)

released from circulation pumping to the borehole fluid (i.e., electrical energy converted by the pump to kinetic energy, and thereafter to thermal energy as hydraulic frictional resistance is overcome) is not considered in the analysis as this paper focuses on heat extraction from the subsurface rocks only. Heat generated from the circulation pump would be expected to be of low significance in hydraulically efficient boreholes, and would also be dependent on pump efficiency. In hydraulically inefficient boreholes, however, heat from circulation pumping may become significant compared with geothermal heat transfer.

In this study, the parasitic power to thermal output ratio (*PPR*) of the system was assessed as the ratio of electrical power (W_{cp}) used during circulation pumping to thermal power ($H_{thermal}$) produced by conductive heat transfer from the surrounding geological formation by the BHE system:

$$PPR = \frac{W_{cp}}{H_{thermal}} \times 100 \quad (30)$$

2.4. Parameterisation, initial and boundary conditions

A linear geothermal gradient of 30 °C/km was used for the initial condition of the simulations, with the temperature of the circulating fluid in the borehole heat exchanger set to the average of the undisturbed geothermal gradient to emulate pre-mixed circulation conditions in the MDBHE prior to the simulation starting. The boundary conditions were set as: i) a fixed constant Dirichlet boundary condition at the surface of 9 °C, ii) Neumann no-flow lateral boundaries (although these were extended to ensure no boundary interaction occurred during the simulation), iii) the basal boundary condition was set as a Neumann boundary, with constant heat flow, which is set to be compatible with the geothermal gradient and rock thermal conductivity—i.e., 75 mW m^{-2} for the base case, equal to 2.5 W/(m K) multiplied by 0.03 K/m, and iv) the inlet for the MDBHE was set as a constant inlet temperature (5 °C). Whilst in real practical operational conditions, a heat load is likely to be imposed on the MDBHE, this study used a constant inlet temperature to identify the differences in specific heat extraction rates.

The model's lateral domain was set to 500 m × 500 m (*x, y*), and the bottom of the boundary was set to have at least 200 m below the depth of the MDBHE (Fig. 3). The spacing around the MDBHE was set based upon the 'mesh-maker tool' by Shao et al. (2016) which provides an optimal spacing around the MDBHE central node using the formula outlined by Diersch et al. (2011b). Time stepping in the simulation was dynamic, and automatically set to increase with time under an automated scheme to ensure numerical convergence. Under base case conditions, universal parameters were assigned with the borehole depth assumed to be 800 m and the borehole parameters assumed are typical of onshore well completions in the United Kingdom (i.e., in line with Banks et al., 2021), albeit with a constant thickness of the surrounding casing. Flow rate was chosen as 5 L/s, based on studies of similar depths which have suggested this is near optimal operating condition for a coaxial DBHE (Kolo et al., 2023). Other parameters are listed in Tables 1 and 2. The parameters listed in the tables are designed to replicate the conditions typical of sedimentary geological settings, whilst a wider range of rock thermal properties were modelled for varied settings. Several parameters can impact the performance of MDBHEs; to evaluate their impact on the hydraulic or thermal performance of different MDBHE types, a range of simulations were conducted. Variable depth, flow rate, rock thermal conductivity, shank spacing, and pipe diameter were all modelled to evaluate their impact on the thermal performance of different MDBHE types.

2.5. Model validation

OGS is an opensource tool that has been tested against data, other modelling software and analytical solutions (e.g., see Shao et al., 2016; Chen et al., 2019; Cai et al., 2021; Brown et al., 2023a,b,c,d; Kolo et al., 2023). Nevertheless, further validation is provided in this paper to continue to rigorously test the capability of OGS as a tool for modelling closed-loop systems. Two examples are provided in this section: 1) a comparison of OGS modelled data to real data provided by Beier et al. (2011) for a shallow U-tube thermal response test and 2) a comparison of OGS modelled data to real data from Acuña and Palm (2013) (with

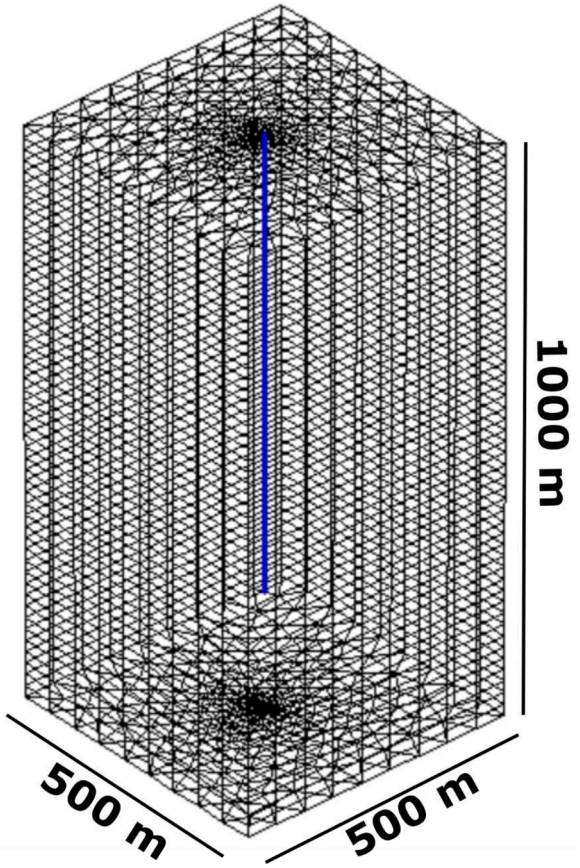

Fig. 3. Example mesh for the base case scenario of an 800 m MDBHE. The blue line highlights the MDBHE.(For interpretation of the references to colour in this figure legend, the reader is referred to the web version of this article.)

Table 2
Base case parameters for different borehole configurations. Note the flow rate for each case is split for the double U-tube, so each pipe has half the flow rate input to the system. The pipes in the U-tube DBHEs were assumed to be made of HDPE.

Parameter	Value	Units
Coaxial (CXA)		
Outer pipe outer diameter	0.1779	m
Outer pipe thickness	0.0081	m
Outer pipe thermal conductivity (steel)	52.7	W/(m K)
Central pipe outer diameter	0.1005	m
Central pipe thickness	0.00688	m
Central pipe thermal conductivity (HDPE)	0.45	W/(m K)
U-tube		
Pipe outer diameter	0.063	m
Pipe thickness (SDR11)	0.00573	m
Pipe thermal conductivity (HDPE)	0.45	W/(m K)
Shank Spacing (pipe centre to pipe centre)	0.12	m
Double U-tube		
Pipe outer diameter	0.063	m
Pipe thickness (SDR11)	0.00573	m
Pipe thermal conductivity	0.45	W/(m K)
Shank Spacing (pipe centre to pipe centre)	0.12	m

data further listed in Beier et al. (2014)) for a shallow coaxial thermal response test.

2.5.1. Comparison to data from a U-tube thermal response test

The data provided in the paper by Beier et al. (2011) are based upon a laboratory sandbox (representative of unconsolidated sand) constructed around a central borehole with an aluminium outer pipe. Parameters for the simulation are listed in Table 3. An average heat input rate of 1056 W was used for the thermal response test and average flow rate of 0.197 L/s. In this study, a variable inlet temperature was adopted as a boundary condition rather than the heat rate, although it has been shown that OGS performs well with a fixed power boundary condition (Brown et al., 2023c). Some parameter values were assumed as they are not provided in the study of Beier et al. (2011). These include: a bulk volumetric heat capacity of 1.9 MJ/m^{3}K for the rock, which is in line with values we may expect from a saturated sandstone (e.g., Banks, 2012), and 1.2 MJ/m^{3}K for the grout. OGS is not capable of modelling the outer aluminium piping, so it was neglected. It is anticipated these minor differences would not impact the results significantly.

The simulation results compared very well with the data from the thermal response test. The outlet temperature from OGS at the end of the simulation was 38.22 °C, which is within 0.15 °C of the data (recorded at 38.07 °C), which represents an error of ~0.4 %. There is a maximum difference of ~0.5 °C in the early time series, but this reduces with time and, as the simulations focus on longer time periods, the impact of this discrepancy will be insignificant on overall results. This is in agreement with past tests by Shao et al. (2016) on older versions of OGS software, albeit with slightly different modelling assumptions (Fig. 4).

2.5.2. Comparison to data from a coaxial thermal response test

A distributed thermal response test for a shallow coaxial borehole heat exchanger was undertaken by Acuña and Palm (2013) for a 188 m long borehole. This test injected heat via downflow through the central pipe (coaxial pipe with centred inlet—CXC configuration) and began recording data at a depth of 17 m. The active length of heat exchange was unknown and therefore, the model comparison developed on OGS started from 17 m with a heat exchange length of 168 m. A fixed power boundary condition (6.36 kW) was used as the input at 17 m on OGS with a constant flow rate of 0.58 L/s. Other parameters are summarised in Table 4. Model results were then compared at 63 h (~3780 min) to the data provided by Beier et al. (2014).

Subsurface data generated from OGS were compared to the distributed thermal response test of Acuña and Palm (2013) at 63 h (Fig. 5). The fluid profiles within the annular space (outlet) and central pipe (inlet) show a proximal fit between the simulations using OGS and the true data, with a maximum discrepancy of less than 0.15 °C. When considering the outlet temperature at 17 m (measured and modelled), there was a percentage error of ~0.6 %.

Table 3
Parameter input from Beier et al. (2011) U-tube thermal response test.

Parameter	Value	Units
Borehole diameter	126	mm
U-tube length	18.3	m
U-tube pipe outer diameter	33.4	mm
U-tube pipe inner diameter	27.33	mm
Shank Spacing (centre to centre)	53	mm
Pipe wall thermal conductivity	0.39	W/(m K)
Ground thermal conductivity	2.82	W/(m K)
Ground volumetric heat capacity	1.9×10^6	J/(K m^3)
Water flow rate	0.197	L/s
Water density	998	kg/m^3
Water volumetric heat capacity	4.179×10^6	J/(K m^3)
Water thermal conductivity	0.59	W/(m K)
Water viscosity	8×10^{-4}	kg/(m s)
Average ground temperature	2 2	°C
Grout thermal conductivity	0.73	W/(m K)
Grout volumetric heat capacity	1.2×10^6	J/(K m^3)

3. Results

In this section, an initial comparison between different types of MDBHE was performed, before a series of parameters were tested to understand their impact on MDBHE performance, in terms of heat extraction, pressure drop and parasitic losses, under different configurations (i.e., coaxial, U-tube and double U-tube).

3.1. Temporal evolution

Initial modelling focused on the performance of base case parameters for each type of MDBHE configuration with a constant inlet temperature boundary condition (5 °C) applied at the top of the borehole and a constant circulation flow rate (5 L/s) for a period of 25 years. All borehole configurations show a rapid decline in the outlet temperature of the MDBHE, with the single U-tube configuration showing the largest drop in temperature and corresponding thermal power. At the end of year 25, the outlet temperature and thermal power for the U-tube configuration were 6.26 °C and 26.3 kW (a depth-average extraction rate of 32.8 W/m), respectively (Fig. 6). In contrast, the coaxial and double U-tube configurations show greater potential in terms of heat extraction from the subsurface store. The coaxial configuration extracts most heat with an end outlet temperature of 6.5 °C, whilst the double U-tube MDBHE has an end outlet temperature of 6.38 °C. Therefore, the corresponding specific (depth-averaged, calculated at the end of the simulation) heat extraction rates were 32.8 W/m (U-tube), 36 W/m (double U-tube) and 39.1 W/m (coaxial). The average specific heat extraction rates for the duration of the simulations were 35.2 W/m (U-tube), 38.8 W/m (double U-tube) and 42.5 W/m (coaxial). It can be inferred that the better heat extraction rates for the coaxial MDBHE are due to a larger surface area of the annular space in contact with the surrounding solid grout/rock and a lower borehole thermal resistance. This is also highlighted in Fig. 6b, where the least heat is drawn into the MDBHE from the U-tube and thus there are colder temperatures in the inlet and outlet pipes. Fig. 7 shows where the ground around the double U-tube and coaxial MDBHE cools significantly quicker than the single U-tube configuration, signifying greater heat extraction.

The coaxial configuration was marginally better than the double U-tube (and significantly better than the single U-tube) in terms of thermal efficiency when extracting heat from the ground, but there are other considerations required for operation, such as cost, engineering practicality, and potential pressure losses (hydraulic resistance) within the MDBHE. When considering the pressure drop in the system, there are far greater losses in the respective U-tube configurations in contrast to the coaxial. In the coaxial design, the pressure drop was recorded as 85 kPa, whilst for the single U-tube and double U-tube configurations the pressure drop was 1.46 MPa and 423 kPa, respectively. The reason for the reduced drop between the U-tube and double U-tube was due to the circulation flow rate being split between the two separate U-tubes within the double U-tube MDBHE. Therefore, it can be observed that coaxial is likely to be the preferred configuration based on the significantly lower pressure losses in contrast to the U-tube configurations. When considering the level of turbulence in the pipe, the Reynolds number can be used to determine the level of turbulent flow. It was established that this number decreases in the coaxial and double U-tubes in comparison to the single U-tube (see Table 5), but that flows are fully turbulent in all cases.

When considering the required power for a circulation pump for each case (with a 100 % efficiency) the coaxial, U-tube and double U-tube would require 0.42 kW, 7.3 kW and 2.11 kW, respectively. If the circulation pump is only 60 % efficient, these figures become 0.71 kW, 12.2 kW and 3.5 kW, respectively. It is recommended in the UK that the pumping power consumption for a closed loop system should be less than 2.5 % of the thermal output (Eq. (30)) (MCS, 2021). It should be

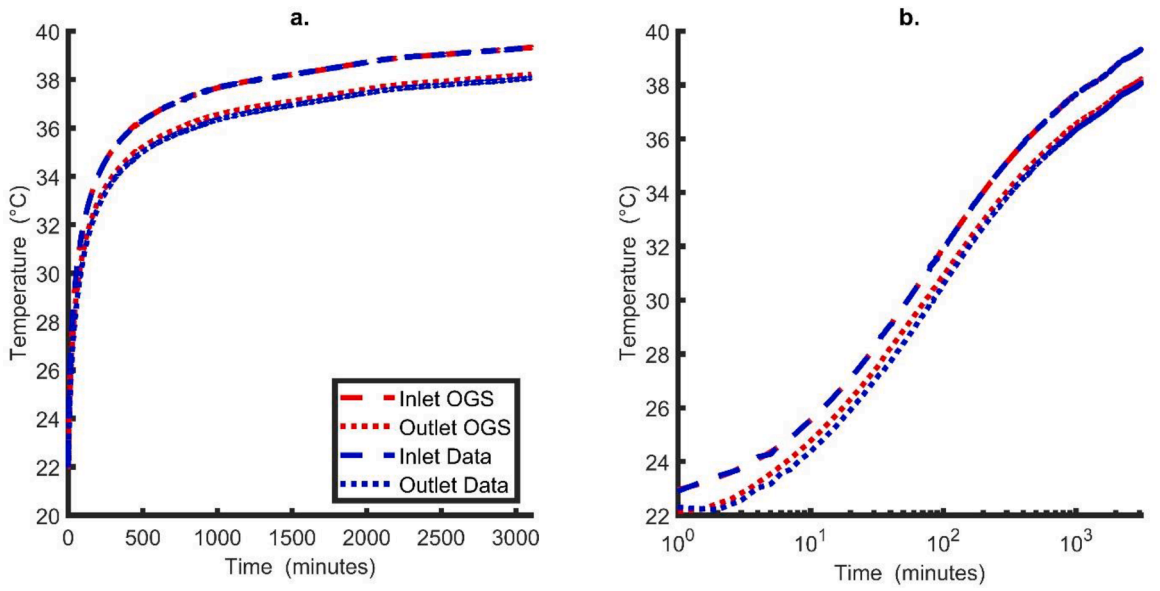

Fig. 4. Inlet versus outlet temperature for the data and OGS simulations plotted on a linear scale (a) and logarithmic scale (b) for the *x*-axis. The red dashed curves show the modelled data from OGS simulation and the blue coded curves depict the experimental data from Beier et al. (2011).(For interpretation of the references to colour in this figure legend, the reader is referred to the web version of this article.)

Table 4
Parameter input from Acuña and Palm (2013) coaxial thermal response test.

Parameter	Value	Units
Borehole diameter	115	mm
Active heat exchanger length	168	m
Internal pipe outer diameter	40	mm
Internal pipe wall thickness	2.4	mm
External pipe outer diameter	114	mm
External pipe wall thickness	0.4	mm
Pipe wall thermal conductivity	0.40	W/(m K)
Ground thermal conductivity	3.25	W/(m K)
Ground volumetric heat capacity	2.24×10^6	J/(K m^3)
Water flow rate	0.58	L/s
Water density	999	kg/m^3
Water volumetric heat capacity	4.19×10^6	J/(K m^3)
Water thermal conductivity	0.59	W/(m K)
Water viscosity	1.138×10^{-3}	kg/(m s)
Heat input rate	6360	W
Average ground temperature	8 .4	°C

noted that the MCS (2021) guidelines are strictly only applicable for small (<45 kW) systems in the UK, and the thermal output is defined as the output of the heat pump rather than the ground loop. Moreover, the circulation pump power should be sufficient to overcome the pressure drop not just in the straight subsurface pipe lengths, but also in bends, fittings, header pipes and the heat pump / heat exchanger. In this study, only the straight subsurface pipe lengths were considered, so our use of this criterion should arguably be far stricter. Nevertheless, of the modelled MDBHE, only the coaxial design sits within this 2.5 % range.

3.2. Impact of depth

Varying depths within the middle-deep range were analysed to test if depth can improve the performance of different configurations of MDBHEs. It was observed that increasing depth resulted in an increase in outlet temperature and thermal power for all borehole configurations recorded at the end of the simulation (Fig. 8a). The difference in thermal power and outlet temperature between the configurations increased with depth.

Similarly, a linear increase in pressure drop was observed which was proportional to depth and of the same order of magnitude (kPa for coaxial configuration and double U-tubes, and MPa for U-tube) (Fig. 9). For depths of 500 m and 1000 m, coaxial MDBHEs showed an increase in pressure drop with depth from 52.9 kPa to 106 kPa, U-tubes showed an increase from 910 kPa to 1.83 MPa, whilst for double U-tubes pressure increased from 265 kPa to 529 kPa. For all cases, pressure drop is proportional to depth, as is predicted by Eq. (28). Eq. (28) assumes a constant viscosity and density: in reality, the viscosity and density will vary with depth in the borehole and also with time, as the system evolves. The greater pressure drop seen in the single U-tube in comparison to the double U-tube is due to the mass circulation flow rate being halved between each U-tube within the double configuration.

Increasing depth also results in a greater requirement of the pumping power because of the high-pressure drops. For depths of 500 m and 1000 m, coaxial MDBHEs require pumping power (assuming a 60 % efficiency) for circulation of 0.44 kW to 0.88 kW, single U-tubes a pumping power of 7.62 kW to 15.2 kW, whilst for double U-tubes pumping power increased from 2.2 kW to 4.4 kW. This highlights that more power is required to extract the thermal energy with increased depths. The PPR decreases with depth (see Table 6), which implies that a higher thermal power can be produced at depth in proportion to the electrical energy consumed.

3.3. Impact of flow rate

Flow rate had a significant impact on both the thermal power and pressure drop. Interestingly, when the flow rate modelled was lowest (1 L/s), the U-tube configuration provided the greatest thermal power recorded at the end of the simulation (Fig. 8b). This was due to greater velocities in the narrower pipes of the U-tube leading to more turbulent flow with greater Reynolds numbers and greater heat extraction (27.1 W/m—recorded at the end of the simulation) in contrast to the other types of MDBHE configuration (7.2 W/m and 22.9 W/m for double U-tube and coaxial, respectively) (see Table 7). It may also be related to the lower surface area of the single U-tube giving less opportunity for thermal short circuiting. The reason for the substantially lower heat extraction rates for the double U-tube configuration was because the flow rate was halved between the two inlets. Greater flow rates (>3 L/s) led to an increase in heat extraction rates for all configurations, with coaxial providing the highest achievable thermal power. Increasing flow rates correlate to a disproportionate increase in pressure drop for all

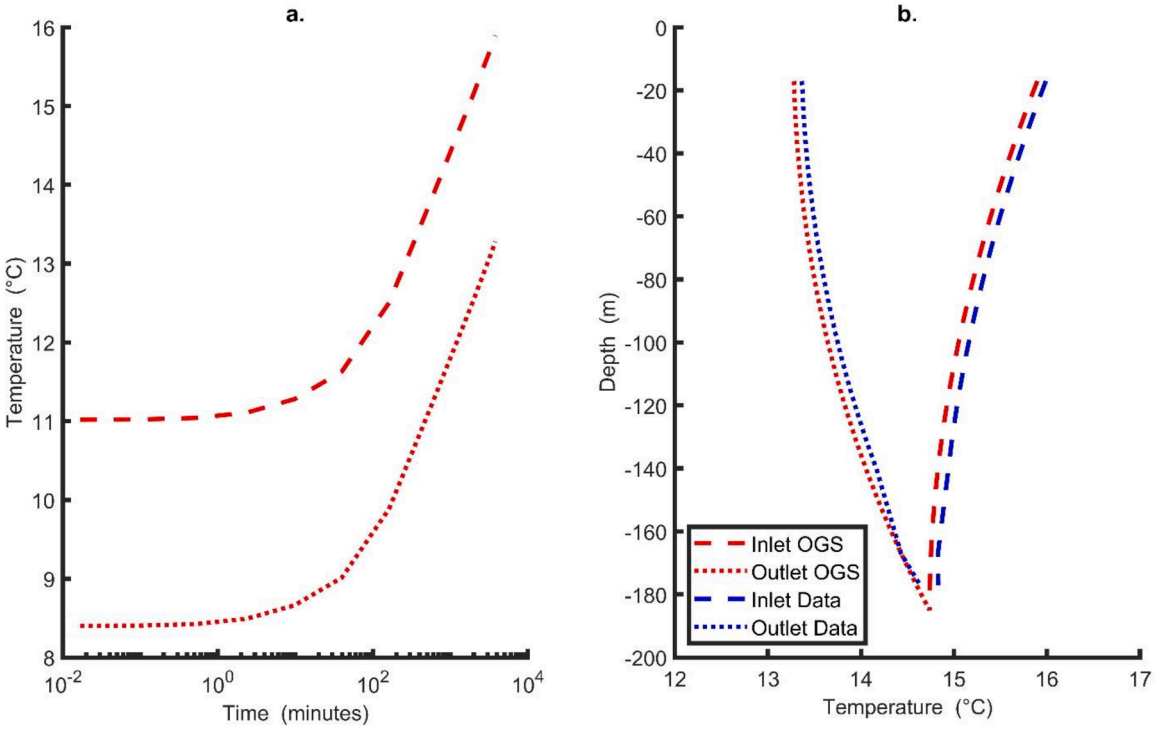

Fig. 5. (a) Inlet vs. outlet temperature from the OGS simulations plotted on a logarithmic scale for the *x*-axis. (b) Comparison of OGS simulations with the experimental data from the distributed thermal response test at 63 h (~3780 min). The red dashed curves show the modelled data from OGS and the blue coded curves depict the experimental data from Acuña and Palm (2013), listed in Beier et al. (2014). Data points at depths over 140 m were extrapolated using plotdigitizer.com.(For interpretation of the references to colour in this figure legend, the reader is referred to the web version of this article.)

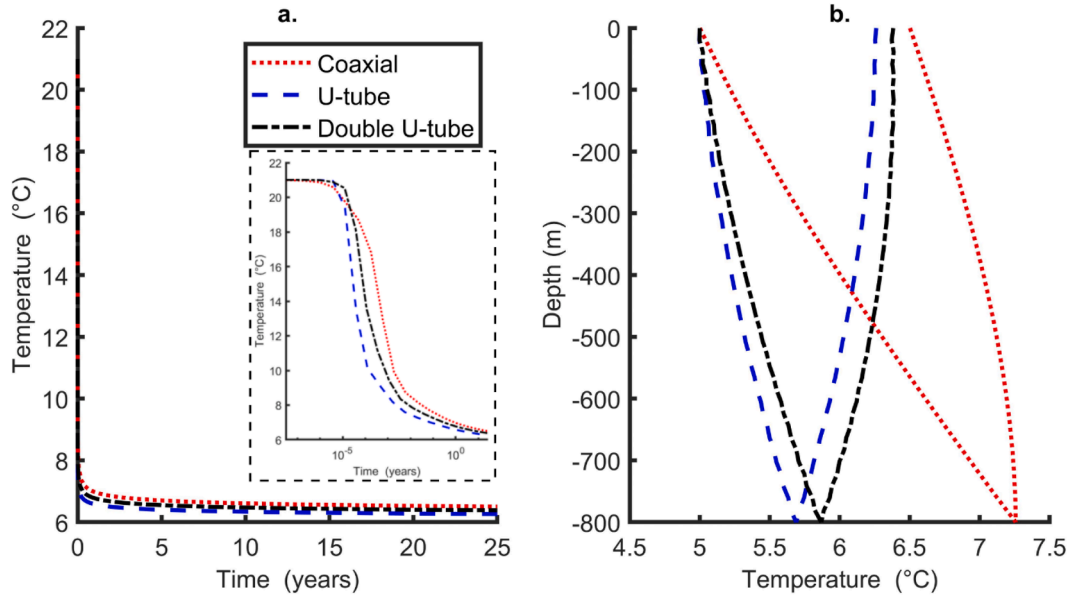

Fig. 6. (a) Outlet temperature decline with time for the different MDBHE configurations and (b) the different fluid temperature within the MDBHE at the end of the simulation plotted against depth. Note that 5 °C is the inlet temperature. Note in figure 'a.' the dashed inset image is the same graph with a logarithmic scale.

MDBHE configuration types (Eq. (28) indicates that pressure loss is proportional to the square of flow rate) (Fig. 10). The U-tube and double U-tube MDBHEs show far higher pressure drops in contrast to the coaxial design. The maximum pressure drop for the largest flow rate (9 L/s) was recorded to be 241.6 kPa (coaxial), 4.22 MPa (U-tube) and 1.21 MPa (double U-tube).

As the pressure drop increased for higher flow rates, so does the power consumption. For the 9 L/s flow rate, the U-tube configuration showed a power use of 63.3 kW, for the double U-tube it was 18.2 kW and for the coaxial configuration it was 3.62 kW. Interestingly, more thermal power was produced, but there was an increase in the electrical consumption to thermal power ratio, for all configurations for higher flow rates (see Table 8). This highlights that the increased energy gained requires a significant proportional increase in electrical energy from increased flow rates. In the case of the maximum pressure (9 L/s) for the U-tube scenario, more electrical energy is required for pumping than

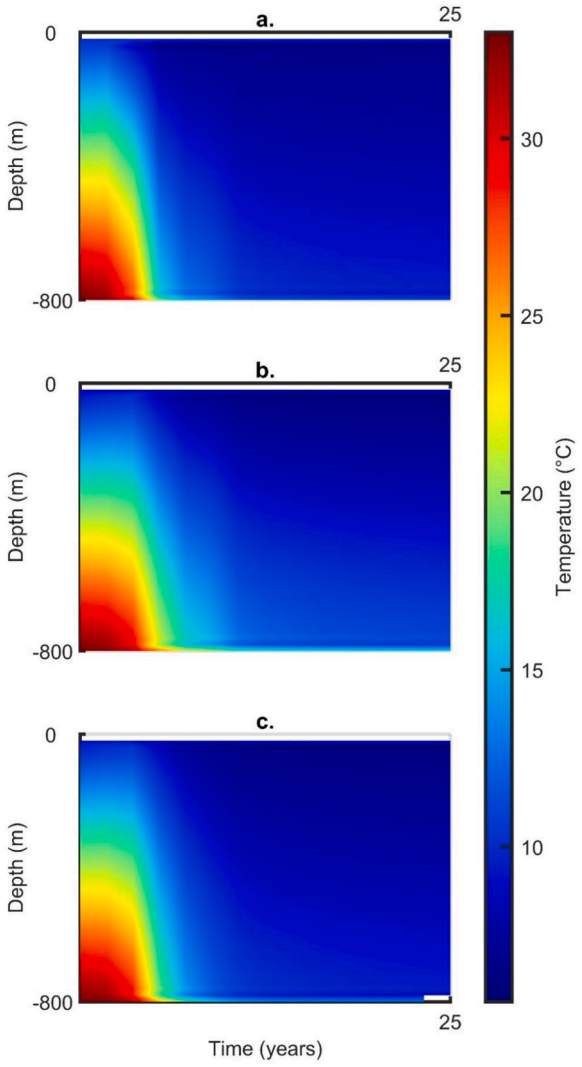

Fig. 7. Thermal evolution of the rock adjacent to the MDBHE with time for following configurations (a) coaxial, (b) U-tube and (c) double U-tube (note that time steps are not uniform and increase with time).

Table 5
Reynolds numbers for different DBHE configurations.

DBHE Configuration	Reynolds number
Coaxial (annulus)	30,289
Coaxial (central pipe)	91,560
U-tube	154,060
Double U-tube	77,030

that gained as a thermal output. Although in all scenarios, the efficiency is poorest for the U-tubes with higher flow rates (Table 8). However, for the lowest flow rate, it is highest in the double U-tubes, due to the reduction in turbulent flow in the double U-tube configuration in comparison to the single.

3.4. Impact of rock thermal conductivity

The rock thermal conductivity of the surrounding formation has a positive near-linear correlation with both outlet temperature and thermal power for all types of heat exchanger. The rate of increase in the U-tube MDBHE is far lower than the other types (Fig. 11), with the maximum rock thermal conductivity of 4.5 W/(m K) corresponding to a thermal power 38.3 kW (47.9 W/m). In contrast, the maximum thermal power and specific heat extraction rate for the coaxial design was 50 kW or 62.5 W/m. As the rock thermal conductivity does not impact the governing equation for pressure, there was no change in pressure drop for any type of MDBHE. Therefore, the efficiency of the system (in terms of electrical energy consumption by the circulation pump to thermal power output) improves with increasing rock thermal conductivity.

3.5. Impact of independent configuration parameters

3.5.1. Shank spacing

Larger shank spacing has been shown to increase the thermal performance of shallow borehole heat exchangers, by reducing the thermal interference between the pipe in and pipe out components of the U-tube (e.g., Vella et al., 2020). This was also the case in the simulations performed in this study where larger spacing for both the single and double U-tube resulted in higher outlet temperatures (and thermal powers) for the duration of the simulation (Fig. 12). The maximum temperatures recorded at the end of the simulation for the single and double U-tubes were 6.26 °C and 6.38 °C, respectively, for the 120 mm spacing. These corresponded to increases in temperature of 0.07 °C and 0.08 °C in contrast to the 90 mm spacing scenario. Therefore, in the modelled scenarios shank spacing was shown to have a small impact on overall performance on the heat extraction rates. The difference in shank spacing for the U-tube resulted in a difference in heat extraction of <1.46 kW (1.82 W/m), whilst for double U-tubes this was <1.67 kW (<2.09 W/m). Under the modelled pressure equation (Eq. (28)) no change was observed between different shank spacing.

3.5.2. Diameter of inner pipe

In this section the diameter of the pipes was varied to understand the impact on performance. To ensure realistic scenarios, the standard dimensional ratio (SDR) was kept at 11 for the U-tubes. This means that borehole wall varies proportionately with diameter, as SDR is defined as the ratio between outer diameter and wall thickness. The difference in thermal performance for varying diameter of the piping for single and double U-tube MDBHEs was minimal. When considering single and double U-tubes, the increase in temperature between the smallest and largest U-tube pipe diameters was 0.098 °C and 0.072 °C, respectively (Fig. 13a). This corresponded to a difference of thermal powers (and specific heat extraction rate) of 2.04 kW (2.55 W/m) and 1.5 kW (1.88 W/m), respectively. Similarly, the diameter of inner pipe for coaxial MDBHEs had a negligible impact on the thermal performance with thermal powers recorded at the end of the simulation showing <0.04 kW difference (Fig. 13b). Smaller internal pipe diameters demonstrate a slightly better thermal performance due to them creating faster velocities in the central pipe resulting in less thermal interference with the outer annular space.

However, the diameter of the piping was more significant in terms of the hydraulic pressure losses in the system. When increasing the inner pipe diameter of the coaxial MDBHE there was a non-linear reduction in pressure loss; for the inner pipe diameter of 98.5 mm and 103.5 mm, the pressure drop was recorded at 89.8 kPa and 78.9 kPa, respectively. Similarly, for the U-tube and double U-tube MDBHEs, the narrower pipe diameters resulted in an increase in pressure drop. For the single U-tube MDBHEs, the pressure drop was recorded at 12.8 MPa (40 mm outer diameter), 4.39 MPa (50 mm) and 1.46 MPa (63 mm), respectively. For the double U-tube MDBHEs, pressure drop was recorded at 3.68 MPa (40 mm), 1.26 MPa (50 mm) and 423 kPa (63 mm), respectively. Therefore, narrower pipe diameters significantly increase the pumping power required (and thus electrical consumption) in comparison to the thermal output (Table 9). Note that our simulation method does not account for heat generated as circulation pumping overcomes frictional resistance—in reality the electricity expended in generating the kinetic energy embodied in circulation pumping would ultimately be converted to heat as frictional resistance is overcome. This would manifest itself as additional useful heat. In a hydraulically efficient borehole heat

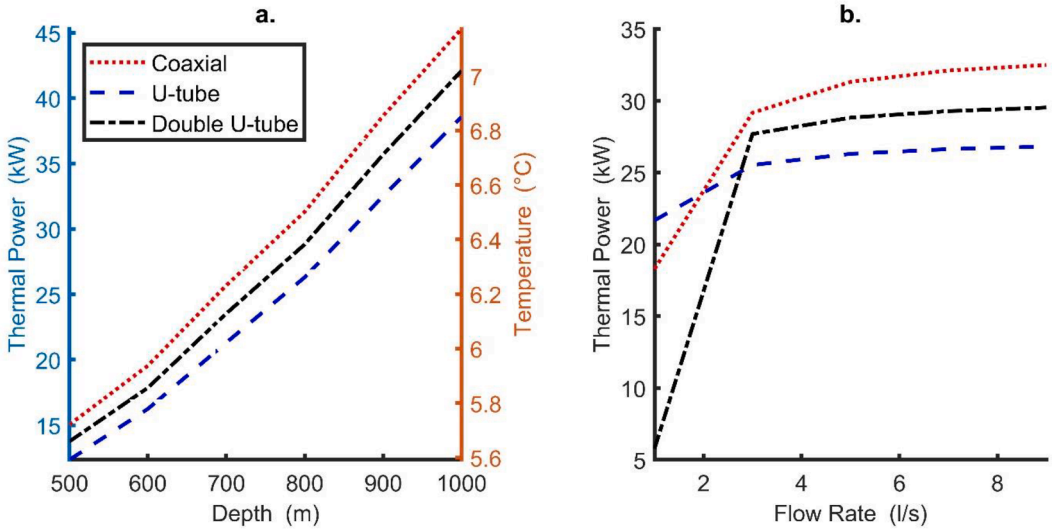

Fig. 8. (a) Recorded end outlet temperatures and thermal powers for varying depths at the end of the 25-year simulation, but keeping flow rate constant at 5 L/s. (b) Varying thermal power for different flow rates recorded at the end of the simulation, keeping depth constant at 800 m.

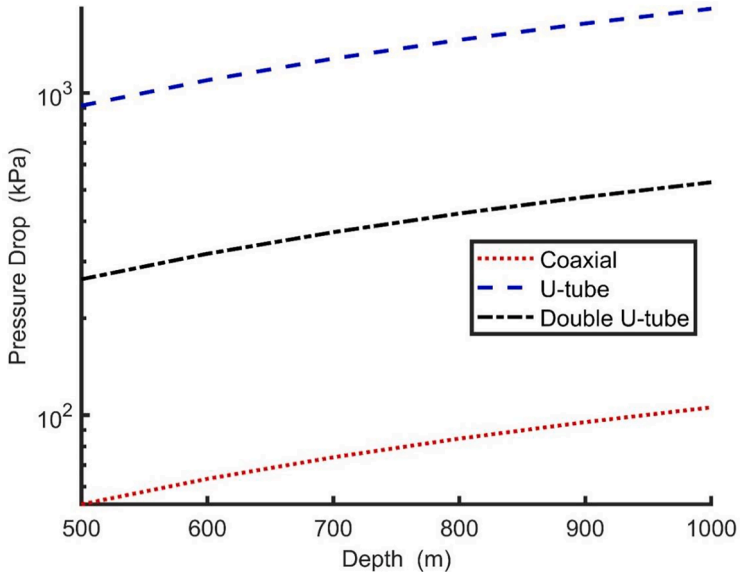

Fig. 9. Pressure drop at varying depths for different MDBHE configurations. Note logarithmic *y*-axis.

Table 6
Different efficiencies of the system (*PPR*) produced for varying depths. Note that thermal power recorded at the end of the simulation. Circulation pump efficiency is assumed to be 60 % in all cases. PPR = parasitic power to thermal output ratio (see Eq. (30)).

MDBHE Configuration	*PPR* (500 m depth)	*PPR* (1000 m depth)
Coaxial	2.93 %	1.95 %
U-tube	61.7 %	39.5 %
Double U-tube	16 %	10.5 %

Table 7
Reynolds numbers for different MDBHE configurations at the minimum and maximum flow rates.

MDBHE Configuration	Reynolds number (1 L/s)	Reynolds number (9 L/s)
Coaxial (annulus)	6058	54,521
Coaxial (central pipe)	18,310	164,810
U-tube	30,810	277,310
Double U-tube	15,410	138,650

exchanger, this would be of low significance in the context of the overall thermal transfer from the geological environment, but could become significant, in a hydraulically inefficient BHE at high values of *PPR*. For the purposes of the modelling in the study, the heat released as a consequence of circulation pumping has been ignored; and thermal yields cited relate to heat conducted from the geological formation to the borehole.

4. Discussion

A range of parameters were tested in this study which revealed that coaxial MDBHEs have a better thermal performance and lower pressure drop in contrast to the other types of heat exchanger (Figs. 14 and 15). The reduction in turbulent flow and pressure drop also leads to lower power consumption of the circulation pump (Fig. 15). When considering the thermal efficiency of a system, in terms of thermal power (kW) or

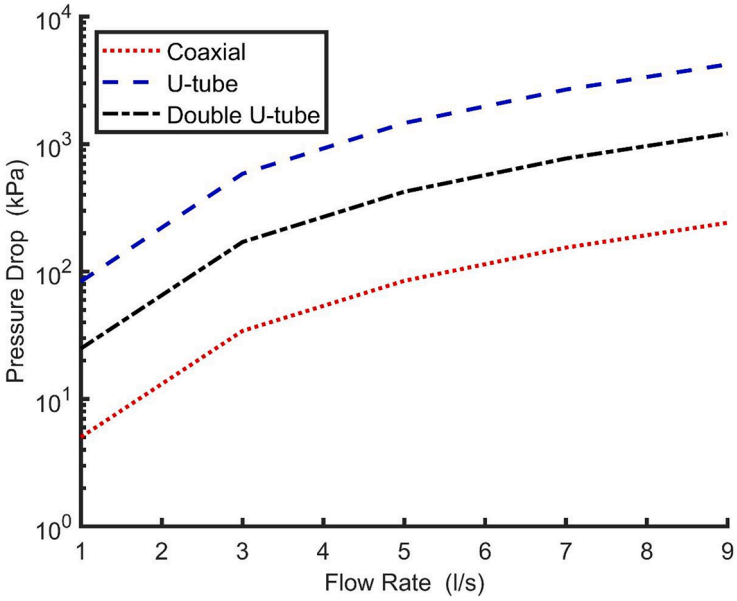

Fig. 10. Pressure drop for varying flow rates for different MDBHE configurations. Note the logarithmic *y*-axis.

Table 8
Different efficiencies of the system (PPR) produced for varying flow rates. Note that thermal power recorded at the end of the simulation. PPR = parasitic power to thermal output ratio (see Eq. (30)).

MDBHE Configuration	*PPR* (1 L/s)	*PPR* (9 L/s)
Coaxial	0.05 %	11.2 %
U-tube	0.64 %	236 %
Double U-tube	0.72 %	61.5 %

specific heat extraction rate (W/m), the double U-tube has a similarly strong performance to the coaxial configuration. Due to the constant inlet temperature method of operation (rather than imposed heat load) and large diameter pipe sizes, shank spacing has minimal impact on the inlet/outlet pipes temperature. This corroborates work undertaken on shallower boreholes and suggests the impact of shank spacing is less pronounced than other parameters such as depth (Vella et al., 2020).

Double U-tubes may be suitable for the middle-deep range for closed-loop borehole heat exchangers in terms of thermal performance. However, they experience far greater pressure drops within the system, almost an order of magnitude higher than the coaxial design, even in comparison to a variety of coaxial pipe inner diameters (Fig. 14). This is likely to make them unfeasible for middle-deep geothermal systems, unless they operate at a reduced flow rate to minimise the pressure drop (although this would, in turn, lead to increased thermal interference and decreased thermal output—Fig. 8). Similarly, single U-tubes result in lower thermal power and the greatest drop in pressure. Furthermore, the increased pressure drop from both U-tube configurations will lead to increased power consumption required in order to circulate the fluid (highlighted for different parasitic power ratios in Fig. 15).

For single and double U-tube MDBHEs, the lowest flow rates (1 L/s) result in significant reductions in pressure drop, so pumping power consumption is minimised putting the MDBHEs within the recommended 2.5 % cut-off for pumping power in comparison to thermal power for ground source heat pumps recommended by MCS (2021). However, these low flow scenarios do represent considerably lower thermal outputs than can be achieved with coaxial configurations at an optimal flow rate (Fig. 8). The higher pressure drop and power

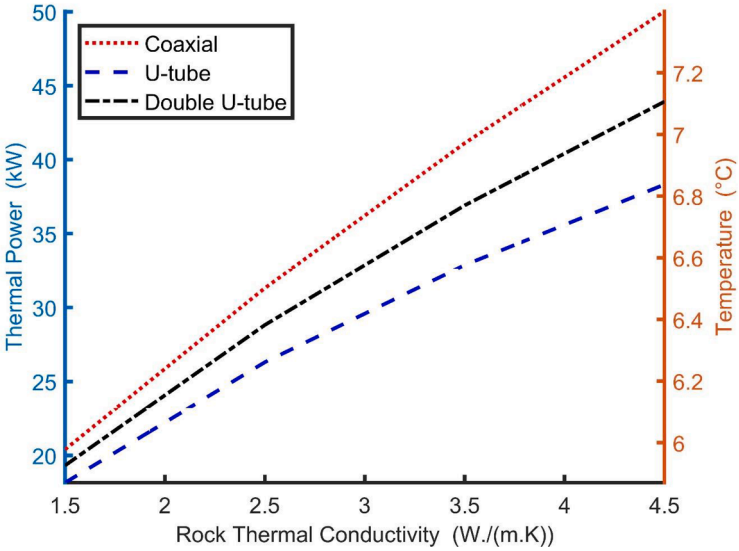

Fig. 11. Thermal power and outlet temperature at end of the 25-year simulation for varying flow rates for different MDBHE configurations.

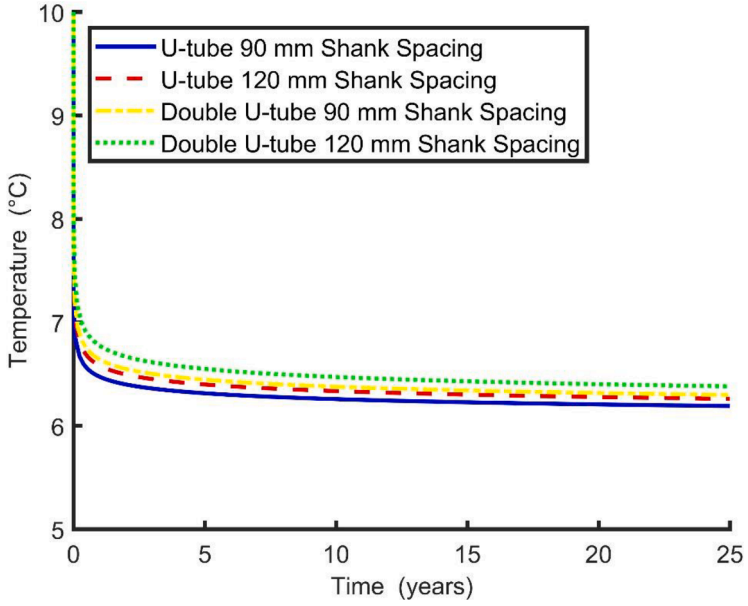

Fig. 12. Outlet temperature for varying shank spacing for U-tube and double U-tube designs. Note that the shank spacing shown is centre to centre of each pipe (see Fig. 2). See Fig. 2 for definition of shank spacing, note value '*s*' is shown here as the distance between tubes diagonally.

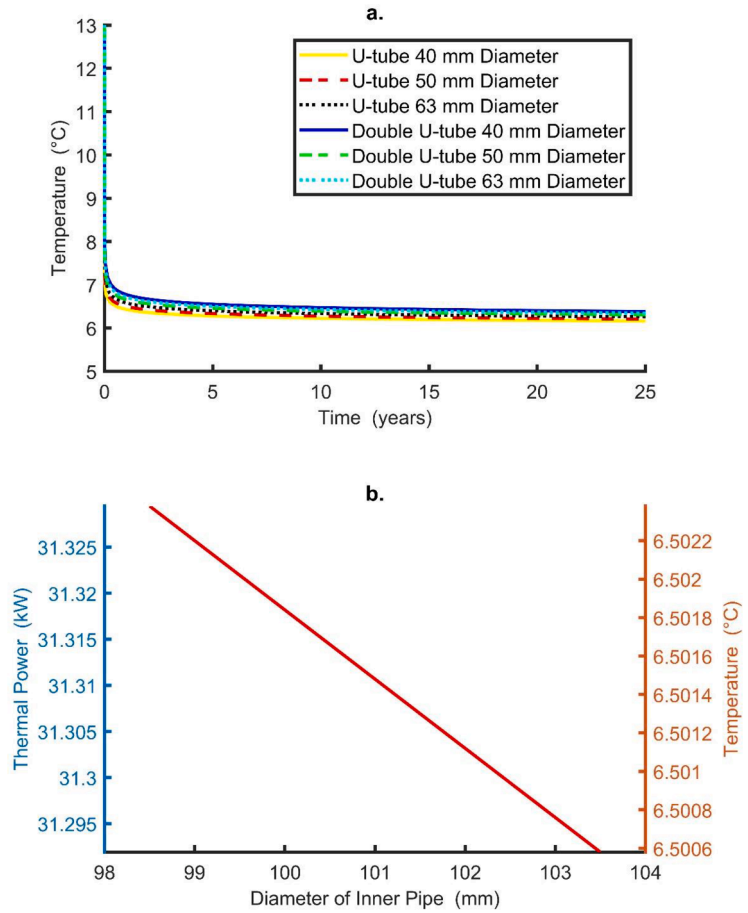

Fig. 13. (a) Outlet temperature at end of the 25-year simulation versus time for varying outer pipe diameters for U-tube and double U-tube designs, while keeping SDR constant at 11. (b) End thermal power and outlet temperature at end of the 25-year simulation for varying central pipe diameter for the coaxial type MDBHE, while keeping the tubing thickness constant.

Table 9
Different ratios of circulation pump power to the thermal power output (PPR) produced for varying U-tube diameters, for a consistent circulation rate of 5 L/s Note that thermal power recorded at the end of the simulation.

MDBHE Configuration	Outer Diameter (mm)	*PPR* (%)
U-Tube	40	440
	50	145
	63	46.3
Double U-Tube	40	110
	50	36.6
	63	12.9

consumption scenarios correspond to high flow rates (>7 L/s) and narrow pipe diameters (<50 mm outer diameter).

Therefore, i) MDBHEs with the single U-tube configuration can only operate with moderate thermal outputs for low flow rates (~1 L/s), which otherwise require significant pumping power, ii) similarly double U-tubes can also only operate under the lowest flow rate (1 L/s) to meet the 2.5 % parasitic power ratio criteria, although generally over all simulations the thermal and hydraulic performance is better than that of the single U-tube, and iii) coaxial MDBHEs are operable under almost any scenario modelled in this paper with acceptable pumping power required. The scenarios where the coaxial system operated slightly above the 2.5 % cut off were at 500–600 m depth, flow rates of 7–9 L/s and finally for the lowest rock thermal conductivity used in the study, due to the decrease in the thermal power produced. The lower depths modelled reduces the thermal output, which means a lower flow rate would be more suitable to meet the parasitic power ratio cut-off. For the higher flow rates the increase in pressure drop requires more circulation pump power. This emphasises the requirement for careful design of MDBHE to DBHE systems to minimise electrical consumption. In general, however, we conclude that co-axial systems are likely to represent the optimum solution for MDBHEs, with high thermal productivity and low hydraulic pressure losses. Finally, there are other practical and economic considerations. The feasibility of installation and total costs may also play an important role in which heat exchanger may be used.

5. Conclusions

In this study, a comprehensive comparison has been made between coaxial, U-tube and double U-tube borehole heat exchangers for middle-deep geothermal systems (500 m to 1000 m). Numerical models were developed using OpenGeoSys software and validated for both U-tube and coaxial systems against data from Beier et al. (2011) and Acuña and Palm (2013), respectively. Model results for both types of borehole heat exchanger showed end outlet temperatures within 0.15 °C and percentage error of <0.6 %. Future work should aim to evaluate and verify the models against empirical data from a real system which is classified as a MDBHE. A range of parameters were then modelled for a period of 25 years using a constant inlet temperature to understand how they impact thermal performance and pressure drop in MDBHEs. The key findings were:

- Coaxial MDBHEs can extract more heat than other types of MDBHEs. For the initial base case, the specific heat extraction rates were calculated at the end of the simulation as 32.8 W/m (U-tube), 36 W/m (double U-tube) and 39.1 W/m (coaxial).
- Coaxial MDBHEs experience far lower pressure drops in contrast to the other types of BHEs. At base case conditions, the coaxial pressure drop was recorded as 85 kPa, whilst for the U-tube and double U-tube configurations the pressure drop was 1.46 MPa and 423 kPa, respectively.
- Increasing depth results in an increase in thermal output, outlet temperature, and pressure drop for all MDBHEs.
- At lower flow rates (1 L/s), U-tube MDBHEs show the best performance in terms of thermal power and specific heat extraction rates. In contrast, thermal short-circuiting is greatest in coaxial BHEs at low flow rates and this is manifested in lower geothermal heat yields. Pressure drop increases with increasing flow rates for all MDBHE types.
- Rock thermal conductivity and shank spacing only impact the thermal performance of MDBHEs. A reduction in shank spacing can lead to thermally inefficient U-tube and double U-tube MDBHEs due to thermal short circuiting, but for the examples presented here the impact of shank spacing is relatively low.
- Single U-tubes are only viable (with PPR values <2.5 %) in the scenario for flow rates of 1 L/s and generally provide low thermal output at depth and offer practical difficulties in installation, thus, highlighting their unsuitability for depths > 500 m due to increased parasitic circulation pumping losses.

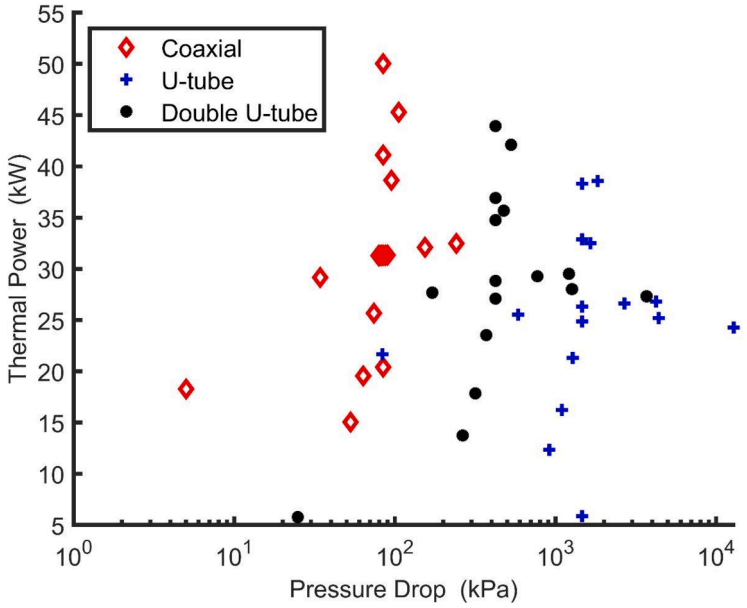

Fig. 14. End thermal power (after the 25-year simulation) plotted against pressure drop for all data of the study for different MDBHE configurations. Note the logarithmic scale of the *x*-axis.

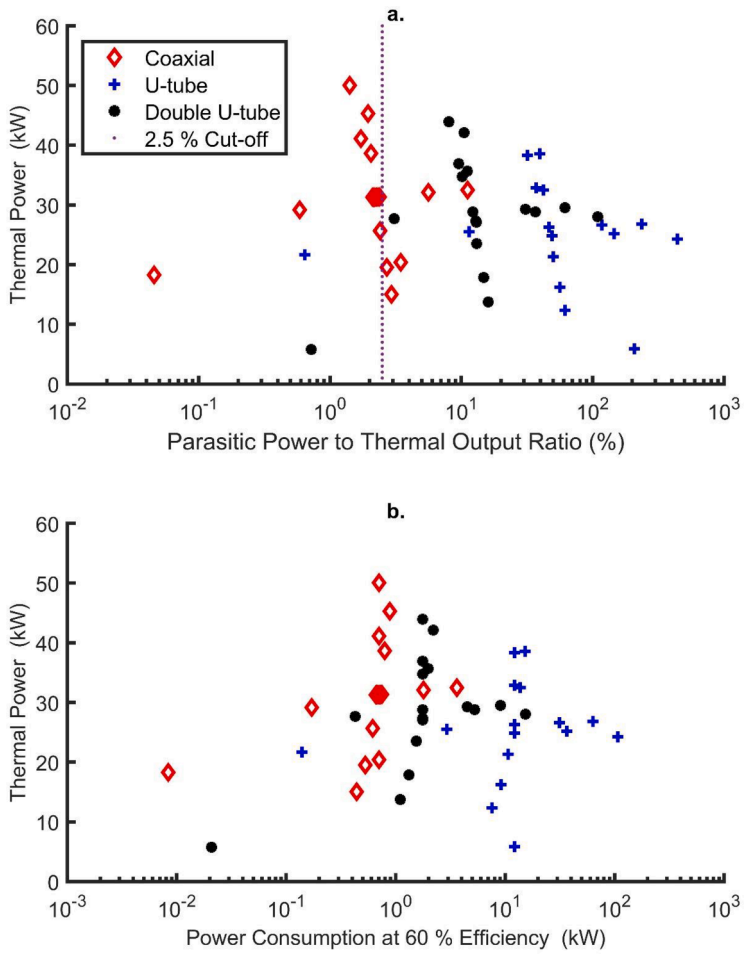

Fig. 15. End thermal power (after the 25-year simulation) plotted against (a) the parasitic power to thermal output ratio and (b) power consumption for a circulation pump efficiency of 60 %. This shows all data of the study for different MDBHE configurations. Note the logarithmic scale of the *x*-axis.

- Double U-tubes only meet the cut-off of 2.5 % parasitic power to geothermal output ratio under the flow rate of 1 L/s and appear to be poorly suited to MDBHE–DBHE systems due to increased parasitic losses. However, they have a significantly reduced pressure drop in contrast to single U-tube MDBHEs. To operate in the MDBHE range either i) the electrical consumption threshold would need to be increased, ii) the borehole diameter should be maximised, or iii) a renewable energy source could contribute to meeting electricity consumption of the heat pump in a hybrid system.
- Coaxial borehole heat exchangers perform best in terms of optimising geothermal heat extraction and minimising hydraulic pressure losses in MDBHEs and DBHEs. Coaxial design should normally therefore be adopted when investigating boreholes at depths greater than 500 m. They are also the only type of MDBHE configuration that meets the MCS (2021) 2.5 % electrical consumption rating in contrast to thermal power output for almost all the simulations, other than those of flow rates of 7 and 9 L/s, depths of 500–600 m and low rock thermal conductivities (1.5 W/(m K)).

CRediT authorship contribution statement

Christopher S. Brown: Conceptualization, Data curation, Formal analysis, Investigation, Methodology, Software, Validation, Visualization, Writing – original draft, Writing – review & editing. **Isa Kolo:** Formal analysis, Methodology, Software, Writing – original draft, Writing – review & editing. **David Banks:** Formal analysis, Supervision, Writing – original draft, Writing – review & editing. **Gioia Falcone:** Funding acquisition, Project administration, Resources, Supervision, Writing – review & editing.

Declaration of Competing Interest

The authors declare that they have no known competing financial interests or personal relationships that could have appeared to influence the work reported in this paper.

Data availability

Data will be made available on request.

Acknowledgements

This work was supported by the UK Engineering and Physical Sciences Research Council (EPSRC) grant EP/T022825/1 and EP/T023112/1. The funding source is for the NetZero GeoRDIE (Net Zero Geothermal Research for District Infrastructure Engineering) and INTEGRATE (Integrating seasoNal Thermal storagE with multiple enerGy souRces to decArobonise Thermal Energy) projects, respectively. For the purpose of open access, the author has applied a Creative Commons Attribution (CC BY) license to any Author Accepted Manuscript version arising from this submission. We would also like to thank two anonymous reviewers and editor for their constructive comments and feedback.

References

Acuña, J., Palm, B., 2013. Distributed thermal response tests on pipe-in-pipe borehole heat exchangers. Appl. Energy 109, 312–320.

Banks, D., 2012. An Introduction to Thermogeology: Ground Source Heating and Cooling. John Wiley & Sons.

Banks, D., 2021. Thermal properties of well construction materials—Newcastle Science Central borehole. *Internal University of Glasgow report for NetZero GeoRDIE project: unpublished*.

Banks, D., 2023. Geothermal heat: status quo or deeper and down? Geoscientist 18. https://geoscientist.online/sections/features/geothermal-heat-status-quo-or-deeper-and-down/.

Bao, L., Wang, X., Jin, P., Cui, J., Zhu, Y., Wang, Y., 2023. An analytical heat transfer model for the mid-deep U-shaped borehole heat exchanger considering groundwater seepage. J. Build. Eng. 64, 105612.

Beier, R.A., Smith, M.D., Spitler, J.D., 2011. Reference data sets for vertical borehole ground heat exchanger models and thermal response test analysis. Geothermics 40 (1), 79–85.

Beier, R.A., Acuña, J., Mogensen, P., Palm, B., 2014. Transient heat transfer in a coaxial borehole heat exchanger. Geothermics 51, 470–482.

Bidarmaghz, A., Narsilio, G.A., 2022. Is natural convection within an aquifer a critical phenomenon in deep borehole heat exchangers' efficiency? Appl. Therm. Eng. 212, 118450.

Breede, K., Dzebisashvili, K., Falcone, G., 2015. Overcoming challenges in the classification of deep geothermal potential. Geotherm. Energy Sci. 3 (1), 19–39.

Brown, C.S., Cassidy, N.J., Egan, S.S., Griffiths, D., 2021. Numerical modelling of deep coaxial borehole heat exchangers in the Cheshire Basin, UK. Comput. Geosci. 152, 104752.

Brown, C.S., Howell, L., 2023. Unlocking deep geothermal energy in the UK, using borehole heat exchangers. Geology Today 39 (2), 67–71.

Brown, C.S., Kolo, I., Falcone, G., Banks, D., 2023a. Repurposing a deep geothermal exploration well for borehole thermal energy storage: implications from statistical modelling and sensitivity analysis. Appl. Therm. Eng. 220, 119701.

Brown, C.S., Doran, H., Kolo, I., Banks, D., Falcone, G., 2023b. Investigating the influence of groundwater flow and charge cycle duration on deep borehole heat exchangers for heat extraction and borehole thermal energy storage. Energies 16 (6), 2677.

Brown, C.S., Kolo, I., Falcone, G., Banks, D., 2023c. Investigating scalability of deep borehole heat exchangers: numerical modelling of arrays with varied modes of operation. Renew. Energy 202, 442–452.

Brown, C.S., Desguers, T., Lyden, A., Kolo, I., Friedrich, D., Falcone, G., 2023d. Modelling borehole thermal energy storage using curtailed wind energy as a fluctuating source of charge. In: Proceedings of the 48th Workshop on Geothermal Reservoir Engineering. Stanford, CA, USA, 6–8 February.

Cai, W., Wang, F., Liu, J., Wang, Z., Ma, Z., 2019. Experimental and numerical investigation of heat transfer performance and sustainability of deep borehole heat exchangers coupled with ground source heat pump systems. Appl. Therm. Eng. 149, 975–986.

Cai, W., Wang, F., Chen, S., Chen, C., Liu, J., Deng, J., Kolditz, O., Shao, H., 2021. Analysis of heat extraction performance and long-term sustainability for multiple deep borehole heat exchanger array: a project-based study. Appl. Energy 289, 116590.

Cai, W., Wang, F., Chen, C., Chen, S., Liu, J., Ren, Z., Shao, H., 2022. Long-term performance evaluation for deep borehole heat exchanger array under different soil thermal properties and system layouts. Energy 241, 122937.

Chen, C., Shao, H., Naumov, D., Kong, Y., Tu, K., Kolditz, O., 2019. Numerical investigation on the performance, sustainability, and efficiency of the deep borehole heat exchanger system for building heating. Geotherm. Energy 7, 1–26.

Diersch, H.J., Bauer, D., Heidemann, W., Rühaak, W., Schätzl, P., 2011a. Finite element modeling of borehole heat exchanger systems: part 1, fundamentals. Comput. Geosci. 37 (8), 1122–1135.

Diersch, H.J., Bauer, D., Heidemann, W., Rühaak, W., Schätzl, P., 2011b. Finite element modeling of borehole heat exchanger systems: part 2, numerical simulation. Comput. Geosci. 37 (8), 1136–1147.

Deng, J., Wei, Q., He, S., Liang, M., Zhang, H., 2019. What is the main difference between medium-depth geothermal heat pump systems and conventional shallow-depth geothermal heat pump systems? Field tests and comparative study. Appl. Sci. 9 (23), 5120.

Doran, H.R., Renaud, T., Falcone, G., Pan, L., Verdin, P.G., 2021. Modelling an unconventional closed-loop deep borehole heat exchanger (DBHE): sensitivity analysis on the Newberry volcanic setting. Geotherm. Energy 9 (1), 1–24.

Engineering Toolbox, 2023. Fluid Flow—Hydraulic Diameter. Accessed on 30/10/23 from: https://www.engineeringtoolbox.com/hydraulic-equivalent-diameter-d_458.html.

Falcone, G., Liu, X., Okech, R.R., Seyidov, F., Teodoriu, C., 2018. Assessment of deep geothermal energy exploitation methods: the need for novel single-well solutions. Energy 160, 54–63.

Fang, L., Diao, N., Shao, Z., Zhu, K., Fang, Z., 2018. A computationally efficient numerical model for heat transfer simulation of deep borehole heat exchangers. Energy Build. 167, 79–88.

Gascuel, V., Raymond, J., Rivard, C., Marcil, J.S., Comeau, F.A., 2022. Design and optimization of deep coaxial borehole heat exchangers for cold sedimentary basins. Geothermics 105, 102504.

Gehlin,S., Andersson, O. & Rosberg, J.E. (2020). Country update for Sweden 2020. Proc. World Geothermal Congress 2020+1, Reykjavik, Iceland, April-October 2021. https://www.geothermal-energy.org/pdf/IGAstandard/WGC/2020/01040.pdf.

Gehlin, S.E.A., Spitler, J. & Hellström, G. (2016). Deep boreholes for ground source heat pump systems—Scandinavian experience and future prospects. Proc. ASHRAE Winter Meeting, Orlando, Florida, January 23–27, 2016. https://media.geoenergicentrum.se/2016/02/Gehlin_et_al_2016.pdf.

Gordon, D., Bolisetti, T., Ting, D.S.K., Reitsma, S., 2017. Short-term fluid temperature variations in either a coaxial or U-tube borehole heat exchanger. Geothermics 67, 29–39.

Harris, B.E., Lightstone, M.F., Reitsma, S., Cotton, J.S., 2022. Analysis of the transient performance of coaxial and U-tube borehole heat exchangers. Geothermics 101, 102319.

Hein, P., Kolditz, O., Görke, U.J., Bucher, A., Shao, H., 2016. A numerical study on the sustainability and efficiency of borehole heat exchanger coupled ground source heat pump systems. Appl. Therm. Eng. 100, 421–433.

Holmberg H., Acuña J., Næss E. & Sønju K.O. (2015). Deep borehole heat exchangers, application to ground source heat pump systems. Proceedings World Geothermal Congress 2015, Melbourne, Australia. 19–25 April 2015.

Holmberg, H., 2016a. Transient Heat Transfer in Boreholes with Application to Non-grouted Borehole Heat Exchangers and Closed Loop Engineered Geothermal Systems. Doctoral thesis 2016:76. Norwegian University of Science and Technology (NTNU), Department of Energy and Process Engineering.

Holmberg, H., Acuña, J., Næss, E., Sønju, O.K., 2016b. Thermal evaluation of coaxial deep borehole heat exchangers. Renew. Energy 97, 65–76. https://doi.org/10.1016/j.renene.2016.05.048.

Homuth, S., Hornich, W., Krenn, H., Sass, I., Spahn, T., 2016. Down-the-hole water-powered hammer drilling method for medium-deep geothermal energy drilling. Oil Gas-European Mag. 42 (1), 39–41.

Incropera, F.P., DeWitt, D.P., Bergmann, T.L., Lavine, A.S., 2007. Fundamentals of Heat and Mass Transfer, sixth ed. John Wiley and Sons.

Infrastructure Act (2015). UK Government legislation: infrastructure Act (2015) explanatory notes. https://www.legislation.gov.uk/ukpga/2015/7/notes. Accessed 19/7/23.

Kohl, T., Salton, M., Rybach, L., 2000. Data analysis of the deep borehole heat exchanger plant Weissbad (Switzerland). In: Proceedings World Geothermal Congress, pp. 3459–3464.

Kohl, T., Brenni, R., Eugster, W., 2002. System performance of a deep borehole heat exchanger. Geothermics 31 (6), 687–708.

Kolo, I., Brown, C.S., Falcone, G., Banks, D., 2022. Closed-loop deep borehole heat exchanger: Newcastle science central deep geothermal borehole. In: European Geothermal Congress.

Kolo, I., Brown, C.S., Falcone, G., Banks, D., 2023. Repurposing a geothermal exploration well as a deep borehole heat exchanger: understanding long-term effects of lithological layering, flow direction, and circulation flow rate. Sustainability 15 (5), 4140.

Korhonen, K., Leppäharju, Hakala, P. & Arola, T. (2018). Simulated temperature evolution of large BTES—case study from Finland. Proc. 2018 IGSHPA Research Conference, Sweden. Doi: 10.22488/okstate.18.000033.

Li, J., Xu, W., Li, J., Huang, S., Li, Z., Qiao, B., Yang, C., Sun, D., Zhang, G., 2021. Heat extraction model and characteristics of coaxial deep borehole heat exchanger. Renew. Energy 169, 738–751.

Liu, J., Wang, F., Cai, W., Wang, Z., Wei, Q., Deng, J., 2019. Numerical study on the effects of design parameters on the heat transfer performance of coaxial deep borehole heat exchanger. Int. J. Energy Res. 43 (12), 6337–6352.

Luo, Y., Xu, G., Zhang, S., Cheng, N., Tian, Z., Yu, J., 2022. Heat extraction and recover of deep borehole heat exchanger: negotiating with intermittent operation mode under complex geological conditions. Energy 241, 122510.

Mazzotti, W., Acuña, J., Lazzarotto, A. & Palm, B. (2018). Deep boreholes for ground source heat pump. Swedish Energy Agency Project 40934-1 Report. Energimyndigheten. http://www.diva-portal.org/smash/get/diva2:1269108/FULLTEXT01.pdf.

MCS, 2021. GSHP hydraulics design guide, chapter 3 in "Heat pump reference information and tools for installers, certification bodies and manufacturers''. MCS Guidance Document MGD 007 ISSUE 1.0. Microgeneration Certification Scheme (MCS) Charitable Foundation, Daresbury, Cheshire, UK. https://mcscertified.com/wp-content/uploads/2021/10/MGD-007-Reference-Information-and-Tools-Issue-1.0.pdf.

Morchio, S., Fossa, M., Beier, R.A., 2022. Study on the best heat transfer rate in thermal response test experiments with coaxial and U-pipe borehole heat exchangers. Appl. Therm. Eng. 200, 117621.

Muovitech (2023). Ground loops turbocollector. Muovitech AB web page, https://www.muovitech.com/UK/?page=products&id=4544, accessed 19/7/23.

Nian, Y.L., Cheng, W.L., Yang, X.Y., Xie, K., 2019. Simulation of a novel deep ground source heat pump system using abandoned oil wells with coaxial BHE. Int. J. Heat Mass Transf. 137, 400–412.

Olsson, J., 2018a. Möjligheter och utmaningar med djupare borrhål *[Possibilities and challenges with deeper boreholes – in Swedish]*. Svensk Geoenergi 2018 (2), 14–16. https://media.geoenergicentrum.se/2018/11/svgeo_2018_02.pdf.

Olsson, J., 2018b. Koaxial en vinnare när Schweiz går på djupet *[Coaxial a winner as Switzerland goes deep – in Swedish]*. Svensk Geoenergi 2018 (2), 17–18. http://media.geoenergicentrum.se/2018/11/svgeo_2018_02.pdf.

Olsson, J., 2018c. Norge: djupare borrning kräver teknikskifte *[Norway: deeper drilling requires different technology – in Swedish]*. Svensk Geoenergi 2018 (2), 20–21. http://media.geoenergicentrum.se/2018/11/svgeo_2018_02.pdf.

Pan, A., Lu, L., Cui, P., Jia, L., 2019. A new analytical heat transfer model for deep borehole heat exchangers with coaxial tubes. Int. J. Heat Mass Transf. 141, 1056–1065.

Perser, I., Frigaard, I.A., 2022. A comprehensive study on intermittent operation of horizontal deep borehole heat exchangers. Energies 15 (1), 307.
Petukhov, B.S., 1970. Heat transfer and friction in turbulent pipe flow with variable physical properties. *In*: Hartnett, J.P. & Irvine, T.F. (eds.) *Advances in Heat Transfer, vol.* 6, 503–564, Elsevier. Doi: 10.1016/S0065-2717(08)70153-9.
Qin, X., Zhao, Y., Dai, C., Wei, J., Xue, D., 2022. Thermal performance analysis on the seasonal heat storage by deep borehole heat exchanger with the extended finite line source model. Energies 15 (22), 8366.
Schulte, D.O., Rühaak, W., Oladyshkin, S., Welsch, B., Sass, I., 2016. Optimization of medium-deep borehole thermal energy storage systems. Energy Technol. 4 (1), 104–113.
SiL (2023). Ecoquartier des Plaines-du-Loup. Web page of City of Lausanne, Services Industriels Lausanne. https://www.lausanne.ch/vie-pratique/energies-et-eau/services-industriels/a-propos-sil/notre-engagement/energies-renouvelables/geothermie/les-plaines-du-loup.html. Accessed 26/4/23.
Shao, H., Hein, P., Sachse, A., Kolditz, O., 2016. Geoenergy Modeling II: Shallow Geothermal Systems. Springer International Publishing, Berlin/Heidelberg, Germany.
Song, X., Wang, G., Shi, Y., Li, R., Xu, Z., Zheng, R., Wang, Y., Li, J., 2018. Numerical analysis of heat extraction performance of a deep coaxial borehole heat exchanger geothermal system. Energy 164, 1298–1310.
Triopipe Geotherm, 2023. Thermex: Installation. Triopipe Geotherm AB. https://www.thermexcollector.com/en/installation. Accessed 19/7/23.
Vella, C., Borg, S.P., Micallef, D., 2020. The effect of shank-space on the thermal performance of shallow vertical U-tube ground heat exchangers. Energies 13 (3), 602.
Wang, J., 2014. Comparative heat transfer efficiency study of coaxial and U-loop boreholes. GSTF J. Eng. Technol. (JET) 2 (4), 1–6.
Wang, Z., Wang, F., Liu, J., Ma, Z., Han, E., Song, M., 2017. Field test and numerical investigation on the heat transfer characteristics and optimal design of the heat exchangers of a deep borehole ground source heat pump system. Energy Convers. Manag. 153, 603–615.
Watson, S.M., Falcone, G., Westaway, R., 2020. Repurposing hydrocarbon wells for geothermal use in the UK: The onshore fields with the greatest potential. Energies 13 (14), 3541.
Wirtén, L., 2017. Geoenergidagen lyfter potentialen *[GeoEnergy day raises potential – in Swedish]*. Svensk Geoenergi 2017 (2), 24–26. http://media.geoenergicentrum.se/2017/11/SvGeo_2_2017-web.pdf.
Wirtén, L., 2018. Hög termisk kortslutning I djupa borrhål *[High thermal short-circuiting in deep boreholes – in Swedish]*. Svensk Geoenergi 2018 (2), 18–19. http://media.geoenergicentrum.se/2018/11/svgeo_2018_02.pdf.
Xia, Z.H., Jia, G.S., Ma, Z.D., Wang, J.W., Zhang, Y.P., Jin, L.W., 2021. Analysis of economy, thermal efficiency and environmental impact of geothermal heating system based on life cycle assessments. Appl. Energy 303, 117671.
Xie, K., Nian, Y.L., Cheng, W.L., 2018. Analysis and optimization of underground thermal energy storage using depleted oil wells. Energy 163, 1006–1016.
Zhao, W., Lei, G., Ma, R., Wang, Z., Song, X., Zhang, J., 2022. A deep geothermal extraction system of three-layer deep borehole heat exchanger for cooling in summer and heating in winter. In: 2nd International Conference on Mechanical, Electronics, and Electrical and Automation Control (METMS 2022), 12244. SPIE, pp. 572–576.
Zhang, W., Li, W., Sørensen, B.R., Cui, P., Man, Y., Yu, M., Fang, Z., 2021. Comparative analysis of heat transfer performance of coaxial pipe and U-type deep borehole heat exchangers. Geothermics 96, 102220.
Zhang, J., Lu, X., Zhang, W., Liu, J., Yue, W., Ma, F., 2022a. Investigation of a novel deep borehole heat exchanger for building heating and cooling with particular reference to heat extraction and storage. Processes 10 (5), 888.
Zhang, F., Fang, L., Zhu, K., Yu, M., Cui, P., Zhang, W., Zhuang, Z., Fang, Z., 2022b. Long-term dynamic heat transfer analysis for the borehole spacing planning of multiple deep borehole heat exchanger. Case Stud. Therm. Eng. 38, 102373.
Zhang, W., Wang, K., Guan, C., Yao, H., Li, W., Gao, Y., Cui, P., 2023. Analysis and optimization of the performance for the ground source heat pump system with the middle-deep U-type well. Appl. Therm. Eng. 219, 119404.